NUMERICAL SIMULATION OF A COUPLED GEOTHERMAL PAVEMENT SYSTEM WITH EVENT-BASED PUMP CONTROL

by

Elvan Keskin

B.S., Civil Engineering, Karadeniz Technical University, 2021

Submitted to the Institute for Graduate Studies in
Science and Engineering in partial fulfillment of
the requirements for the degree of
Master of Science

Graduate Program in Civil Enginnering
Boğaziçi University
2025

ACKNOWLEDGEMENTS

I would like to express my earnest gratitude to my supervisor, Prof. Dr. Özer Çinicioğlu, for their insightful guidance, unfaltering support, and patience. His everlasting assistance, vast knowledge, and kindness were essential to the success of this thesis.

I am grateful to my colleagues Mert Güner and Uğur Can Erginağ for their assistance in my work, their valuable contributions, and their gratifying generosity. A special thanks goes as well to my colleagues in Office 164. Throughout this journey, they lifted me up every time I fell, believed in me when I lost hope in myself, guided me toward the right path time and again, and put a smile on my face even in moments I thought were impossible. I couldn't have imagined better companions along the way.

Beyond everything, I am forever thankful to my mom, Emine Yazıcı, and siblings, Muhammet, Ömer Faruk, and Zühre Ay Keskin, for always trusting my abilities, inspiring me to keep going, and rewarding me with their priceless love. Nothing would be possible without their presence in my life. Everything I achieve is due to my mother's sacrifices and the support of my siblings.

Lastly, I dedicate this study to all women in STEM. This patriarchal world often seeks to undermine us, betray our intelligence, or ignore our voices, but we will continue to claim our rightful place in academia and beyond. Being a woman in this field is one of the greatest honors that could be achieved and is a tribute to the countless women before us who had the minds of scientists and scholars but were denied, silenced, or persecuted for daring to think differently. We owe it to them and to ourselves to continue to push forward.

ABSTRACT

NUMERICAL SIMULATION OF A COUPLED GEOTHERMAL PAVEMENT SYSTEM WITH EVENT-BASED PUMP CONTROL

The increasing global demand for energy has led to a growing interest in sustainable energy sources. The utilization of geothermal energy presents a promising alternative to meet this demand due to its accessibility and unlimited nature. Among the various applications of geothermal energy, one innovative use is de-icing pavement systems. This study aims to investigate the performance of a geothermal pavement system under winter conditions through a numerical simulation using COMSOL Multiphysics. An energy pile is connected to the pavement via a closed-loop pipe network. In order to prevent ice formation on the pavement surface, the heat carrier pipes transfer heat from the ground to the pavement through a circulating fluid. The coupling of Heat Transfer in Porous Media, Heat Transfer in Pipes, and Pipe Flow physics helps simulate more realistic thermal and fluid dynamics. The surface boundaries include environmental factors such as solar radiation, wind, and latent heat transfer. The pump operation was controlled on the basis of the pavement surface and ambient temperatures using the Events interface. The traditional approach is to study the pavement and energy pile separately, which overlooks the effect of the inter-domain heat transfer. This work offers a unified approach through a coupled system, enhancing the accuracy of performance assessment.

ÖZET

KOŞULA BAĞLI POMPA KONTROLÜ UYGULANAN BİRLEŞTİRİLMİŞ JEOTERMAL YOL YÜZEYİ SİSTEMİNİN SAYISAL SİMÜLASYONU

Artan küresel enerji talebi, sürdürülebilir enerji kaynaklarına olan ilgiyi artırmıştır. Jeotermal enerjinin kullanımı, erişilebilirliği ve tükenmez doğası sayesinde bu talebi karşılamak için etkin bir alternatif sunmaktadır. Jeotermal enerjinin çeşitli uygulamaları arasında, yenilikçi bir kullanım alanı da kaldırım sistemlerinin buzdan arındırılmasıdır. Bu çalışma, kış koşullarında bir jeotermal kaldırım sisteminin performansını değerlendirmek amacıyla COMSOL Multiphysics yazılımı kullanılarak sayısal bir simülasyon gerçekleştirmeyi amaçlamaktadır. Bir enerji kazığı, yol yüzeyine kapalı devre boru ağı aracılığıyla bağlanmıştır. Yol yüzeyinde buz oluşumunu önlemek amacıyla, ısı taşıyıcı borular dolaşan bir akışkan vasıtasıyla yer altından yol yüzeyine ısı transferi sağlamaktadır. Heat Transfer in Porous Media, Heat Transfer in Pipes ve Pipe Flow fizik modüllerinin birlikte kullanımı, daha gerçekçi bir ısıl ve akışkan dinamiği simülasyonuna olanak tanımaktadır. Yüzey sınırlarında güneş radyasyonu, rüzgar ve gizli ısı transferi gibi çevresel faktörler modele dahil edilmiştir. Pompa çalışması, yol yüzeyi ve ortam sıcaklıklarına bağlı olarak Events arayüzü ile kontrol edilmiştir. Geleneksel yaklaşımda yol yüzeyi ve enerji kazığı ayrı ayrı incelenmekte olup, bu durum hacimler arası ısı transferinin etkisini göz ardı etmektedir. Bu çalışma ise, bu iki bileşeni kapalı devre bir sistemle birleştirerek hacimler arası ısı etkileşimini dikkate alan birleşik bir model sunmakta ve performans değerlendirmesinin doğruluğunu artırmaktadır.

TABLE OF CONTENTS

LIST OF FIGURES

LIST OF TABLES

LIST OF SYMBOLS

A	Cross-sectional or surface area (m^2)
C_p	Specific heat capacity at constant pressure
C_{ps}	Heat capacity of snow
d_h	Hydraulic diameter of the pipe
e_t	Tangential unit vector
f_D	Darcy friction factor
h	Convective heat transfer coefficient
h_{ext}	Convective heat transfer coefficient on the external surface of the pipe
h_{int}	Convective heat transfer coefficient on the internal surface of the pipe
$(hZ)_{\text{eff}}$	Effective heat transfer coefficient per unit length
H_f	Latent heat of fusion of snow
I	Direct radiation on a horizontal surface
k	Thermal conductivity
k_{eff}	Effective thermal conductivity of the porous medium
$k_{\text{wall},n}$	Thermal conductivity of the n-th wall layer
m	Mass snowfall rate
m_{pump}	Mass flow rate of the pump
Nu	Nusselt number
Q	Volumetric/general heat source
Q_{geo}	Geothermal heat source
Q_p	Work done by pressure forces
Q_{vd}	Viscous dissipation
q	Rate of heat transfer
q_{conv}	Convective heat flux
q_o	Heat flux needed to melt snow
q_{rad}	Infrared radiation heat flux
q_{solar}	Solar radiation heat flux

q_s	Heat flux under snow
r_n	Outer radius of the n-th wall layer
r_{n-1}	Inner radius of the n-th wall layer
t	Time
T	Temperature
T_{ext}	Temperature of the external domain
T_f	Fluid temperature
T_m	Melting temperature
T_{sky}	Sky temperature
T_s	Surface temperature
T_{snow}	Snow temperature
u	Fluid velocity
u_{in}	Average velocity at the inlet
u_{out}	Average velocity at the outlet
Z_0	Internal wetted perimeter of the pipe
Z_N	External wetted perimeter of the pipe

α	Absorptivity coefficient
α_{irr}	Surface absorptivity
ϵ	Surface emissivity
μ	Dynamic viscosity
ρ	Density of fluid or material
σ	Stefan-Boltzmann constant
σ_{SB}	Alternate notation for Stefan-Boltzmann constant

LIST OF ACRONYMS/ABBREVIATIONS

1D	One-dimensional
2D	Two-dimensional
3D	Three-dimensional
ANN	Artificial Neural Networks
BTES	Borehole Thermal Energy Storage
COP	Coefficient of Performance
FEM	Finite Element Models
GSHP	Ground Source Heat Pumps
KNN-ML	K-Nearest Neighbor Machine Learning
TRT	Thermal Response Test
UHI	Urban Heat Island

1. INTRODUCTION

Sustainable energy sources have gained interest due to the increase in global energy demand. Among these, geothermal energy presents a promising solution, offering both environmental and economic advantages. Ground source heat pumps (GSHP), thermo-active energy piles, and borehole thermal energy storage (BTES) systems are among the most widely used geothermal technologies.

Recently, an innovative application of geothermal energy has gained attention. Geothermal pavements are utilised in order to provide an alternative to the traditional de-icing methods. Salting and the use of electrical resistance heaters have been the most common operations against the formation of ice over the pavement surface, but these methods are environmentally damaging and economically inefficient.

Geothermal pavement systems include an energy pile and a set of horizontal heat exchanger pipes embedded beneath the surface of the pavement, at a shallow depth of 1 to 2 meters. An energy pile is a conventional foundation pile with heat exchanger pipes integrated, typically to the steel reinforcement cage. These pipes form a closed-loop system, linking the energy pile with the pavement surface. A circulating fluid, commonly water,transfers heat from the ground to the pavement, mitigating surface ice formation during winter.

In this study, a numerical simulation of a geothermal pavement system was performed in COMSOL Multiphysics Software to evaluate the efficiency of heat transfer to the pavement surface in winter conditions. A cylinder, representing the ground, was modelled. On the surface of the ground, a block was modelled as a part of the geothermal pavement. At the centre of the ground, another cylinder was located and assigned as a borehole. Heat exchanger pipes were modelled as 1D elements. In the borehole, the pipes were in a single U-shaped configuration, and in the pavement, a serpentine configuration was used.

In order to simulate the heat exchange between the domains, the Heat Transfer in Porous Media and the Heat Transfer in Pipes physics modules were employed. The Pipe Flow module couples fluid dynamics with heat transfer. Initial and boundary conditions were assumed based on real-life data. The far-field and bottom boundaries were assumed to be adiabatic with no heat transfer. At the surface of the pavement and the ground, solar radiation, solar gain, wind, and latent heat transfer were incorporated to enhance the model's realism.

To simulate realistic system behaviour, the Events interface in COMSOL was used to control the operation of the heat pump based on surface conditions. The pump is activated when the pavement surface temperature drops below 7℃ and deactivated when it reaches 9℃. This operation is used to prevent the formation of ice and dew on the pavement surface. Additionally, the system is designed to minimise its contribution to the urban heat island effect. To achieve this, the pump also activates when the pavement surface temperature rises 10℃ above the ambient air temperature and stops once it reaches ambient conditions.

This study provides a comprehensive approach to modelling geothermal pavement systems. Traditionally, the pavement and the energy pile are uncoupled and modelled separately. However, such an approach neglects the heat transfer interactions between the domains. This work addresses that limitation by integrating the pavement and energy pile within a unified model connected through a closed-loop heat exchanger system, thereby more accurately reflecting real-world thermal behaviour.

2. LITERATURE REVIEW

2.1. Geothermal Energy

Geothermal energy is defined as the heat stored in Earth's core. The source of this heat is the planet's formation 4.5 billion years ago and the radioactive decay of naturally occurring radioactive isotopes. It is considered a renewable energy source because the heat derived from the Earth's crust is limitless. The utilization of geothermal energy dates back to the Paleolithic age, as hot springs were used in daily life for washing, cooking, and bathing. [1] As the demand for sustainable energy resources increased, geothermal energy became the focus of new studies, and many developments in this field were achieved. Throughout the world, about 8200 MW of electricity is produced from geothermal energy power plants. [2]

The temperature and thermal properties of the Earth are the most important parameters that affect heat transfer. The temperature of a specific location can be observed through field tests, but the general temperature distribution for various sites is available in the literature. [3] Kusuda states that the temperature of the ground below approximately 6 m (20 ft) is relatively stable. Above this level, the temperature is sensitive to atmospheric conditions. Heat from the Earth's core moves towards the crust and dissipates. Thus, as depth increases, the temperature of the ground also increases. [4]

2.2. Geothermal Energy Extraction

Geothermal energy can be directly used for different applications such as space heating, commercial treatment, greenhouse heaters, and traditional bathing practices. Direct use of geothermal energy depends on currently available technology and basic engineering principles. [5] The decrease in reserves, rise in operational costs and oil prices, and sustainable energy demand led the energy industry to explore and utilize these clean and cheaper energy sources. Utilization of geothermal energy occurs through geothermal systems. Geothermal systems are commonly classified depending on their exploitation depths. Systems with operational depths greater than 400 m are considered deep geothermal systems, while those operating at depths less than 400 m are classified as shallow geothermal systems. Three main components make up geothermal systems: a heat source (typically the ground), a heat sink (typically the built environment), and a heat exchanger (generally pipes containing fluid).

Shallow geothermal systems, because of their low operational depths, harness geothermal energy indirectly. Additional devices are employed to enhance or lower the energy transferred between the heat source and heat sink. These systems are adequate for small-scale and domestic applications. They can be utilized to provide space heating, cooling, and hot water using underground temperatures less than 25℃. On the other hand, in deep geothermal systems, direct use of geothermal energy is possible. Additional devices are not necessary in this case, except for controlling the flow of the heat exchanger fluid. These systems are generally employed for medium- to large-scale operations, exploiting underground temperatures greater than 25℃ and up to 200℃. They can be utilized to provide heating and hot water, as well as electrical power.

Another classification of geothermal energy systems is based on the presence of closed- or open-loop heat exchangers. Systems that employ sealed pipes containing heat exchanger fluid are considered closed-loop systems. Open-loop systems involve the direct use of groundwater from aquifers through wells. In these systems, mass exchange occurs, enhancing heat transfer efficiency. However, despite exploiting a greater amount of energy, open-loop systems are less cost-efficient and prone to environmental risks such as underground pollution. Closed-loop systems minimise such risks and do not require extractive licensing. Shallow geothermal systems can employ open- or closed-loop heat exchange, whereas deep geothermal systems are generally open-loop.

Typical examples of shallow geothermal systems include horizontal geothermal boreholes, geothermal baskets, groundwater capture systems, vertical geothermal boreholes, and energy geostructures. Common examples of deep geothermal systems include thermal springs, hydrothermal systems, and petrothermal systems. [6]

2.3. Thermoactive Geostructures

Thermoactive geostructures, commonly known as energy geostructures, are a developing and versatile technology that can be used for structural and energy transfer applications. All structures embedded in the ground that exchange heat with it while providing structural support are considered thermoactive geostructures. Examples of thermoactive geostructures include those using deep foundations, such as piles, piers, and barrettes; shallow foundations, such as footings and base slabs; earth-retaining structures, such as diaphragm walls and sheet pile walls; as well as tunnel linings and anchors.

Thermoactive geostructures can function for multiple objectives. Energy piles, energy walls, energy slabs, and energy tunnels can be used for heating and cooling superstructures. They can be employed to produce hot water for anthropogenic purposes. Energy piles that support bridge piers, energy slabs, and energy pavements can provide heat for deicing the pavements and bridge decks of roads, bridges, station platforms, and airport runways. Heat can be stored in the ground for consecutive use via energy piles, energy walls, energy slabs, and energy tunnels.

2.3.1. Materials

Generally, concrete is chosen as a medium because of its favorable thermal conductivity and thermal storage capacity. [7] Thermoactive geostructures contain pipes embedded within the reinforced concrete. In shallow and closed-loop geothermal systems, a heat exchanger fluid flows through these pipes. This fluid can be water or a water-antifreeze solution. Generally, ethylene glycol and propylene glycol are employed as antifreeze additives. Heat exchanger pipes are usually made of high-density polyethylene. In order to optimise energy efficiency, the first meters of the pipes are insulated to prevent the effects of climatic conditions. Heat exchanger boreholes with diameters of 10–15 cm are drilled to depths of 20–300 m. A large number of boreholes can be employed in a system with appropriate separation to limit performance degradation. [8]

The configuration of heat exchanger pipes embedded into the concrete has an impact on the efficiency of energy production and the cost of operation. Different configurations, such as single-U-shaped, multi-U-shaped, W-shaped, and spiral, have been employed. Spiral and W-shaped pipe configurations have higher efficiency, while the U-shaped is the most cost-efficient configuration. [9]

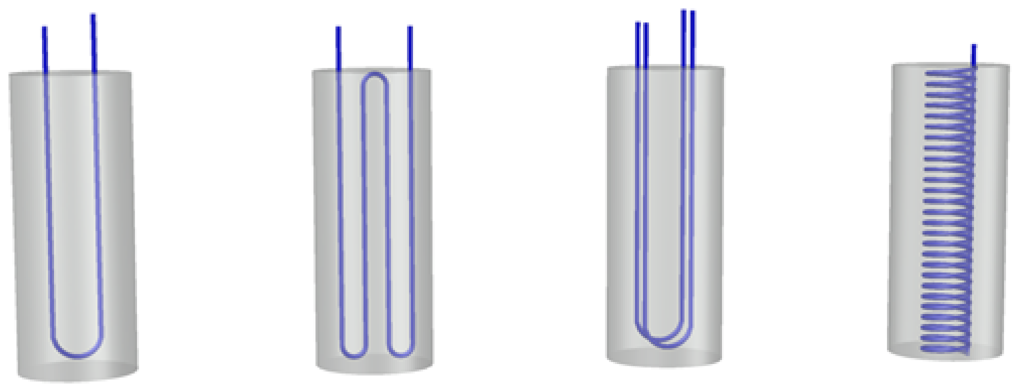

Figure 2.1. Schematics of pipe configurations in energy piles: single-U, W, multi-U, and spiral.

When dealing with energy pavements, pipe configurations such as series, unbalanced ladder shape, balanced ladder shape, and parallel can be considered. [10] The most commonly used type is the series configuration. This configuration is illustrated in Figure 2.2. When designing the pipe configuration of energy geostructures with significant heat exchange surfaces, the goal is to maximize heat exchange while minimizing pressure drop and investment costs.

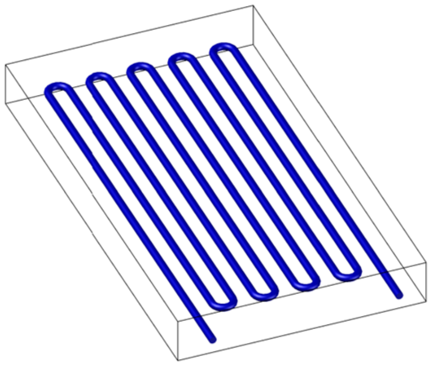

Figure 2.2. Series pipe configuration in energy pavements.

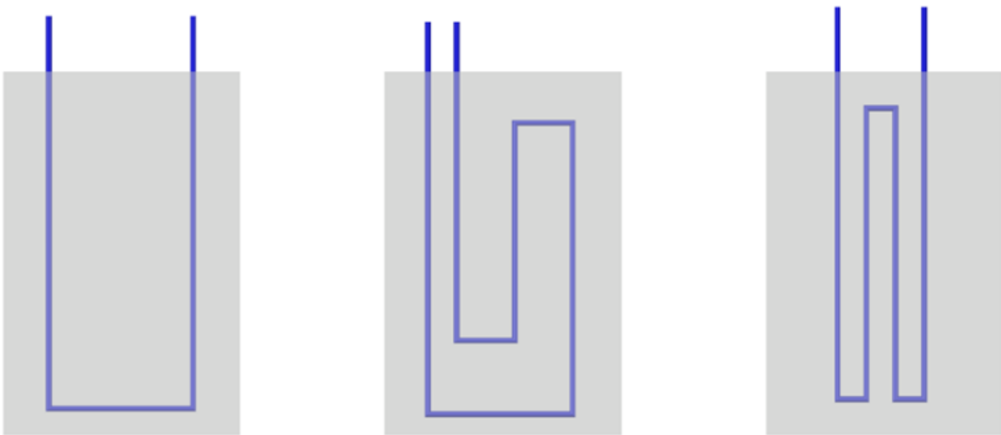

Figure 2.3. The schematics of the pipe configurations in energy walls.

The efficiency of the systems also depends on the heat exchange interfaces. Energy tunnels, walls, slabs, and pavements have both air–solid and solid–solid heat exchange interfaces. The selection of an appropriate pipe location has a considerable influence on the heat exchange between these interfaces.

2.3.2. Operating Systems

Thermoactive geostructures use the ground as a heat source in winter and a heat sink in summer for heating and cooling purposes. The temperature of the ground within a few meters of the surface is close to the ambient temperature and is greatly influenced by meteorological changes. However, as depth increases, the ground temperature becomes almost constant and is close to the mean atmospheric temperature. The average thermal gradient varies with depth and is about 25℃ to 30℃ per kilometer due to heat generation within the crust. [11] Thus, the ground is warmer than the ambient temperature during cold seasons and colder during warm seasons.

Thermoactive geostructures contain two main circuits connected by a ground source heat pump. The two main circuits are the primary circuit and the secondary circuit. Figure 2.4 illustrates this configuration. The primary circuit exchanges heat with the ground via the selected heat carrier fluid flowing through the pipes embedded in the geostructure. The superstructure is cooled or heated via the secondary circuit. When the heat carrier fluid enters the heat pump and passes through the compressor, it is compressed and becomes warmer. When the fluid passes through the evaporator, it expands and cools. This operating principle is reversed in heat pumps that operate in cooling mode.

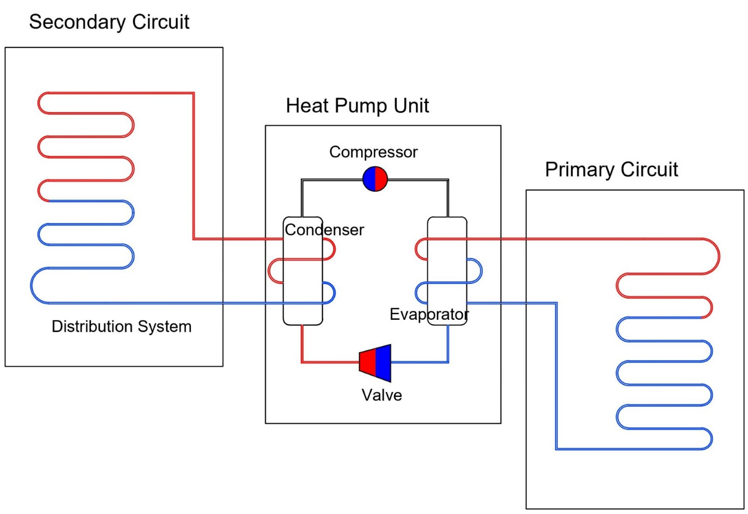

Figure 2.4. Schematics of a geothermal source heat pump system.

It is desirable for the heat pump to be both ecologically and economically efficient. Efficiency is characterized by the coefficient of performance (COP). EN 14825 defines COP as the ratio of the declared heating capacity of the unit to the effective power input of the unit at a specific temperature condition. [12] A higher coefficient of performance corresponds to greater efficiency. COP is expressed as

$$\text{Coefficient of Performance} = \frac{\text{Delivered Energy (kW)}}{\text{Input Energy (kW)}}. \tag{2.1}$$

2.4. Modes of Heat Transfer

Heat transfer occurs between two particles that have different temperatures. Heat is transferred by three modes: conduction, convection, and radiation. For energy geostructures, it flows mainly by conduction and convection. [13] A schematic illustrating the heat transfer modes occurring in energy geostructures is shown in Figure 2.5. Heat transfer by convection can be minimized via thermal insulation between energy geostructures and the underground environment. The heat exchange mechanism that occurs between the ground and the energy geostructure is illustrated in Figure 2.6.

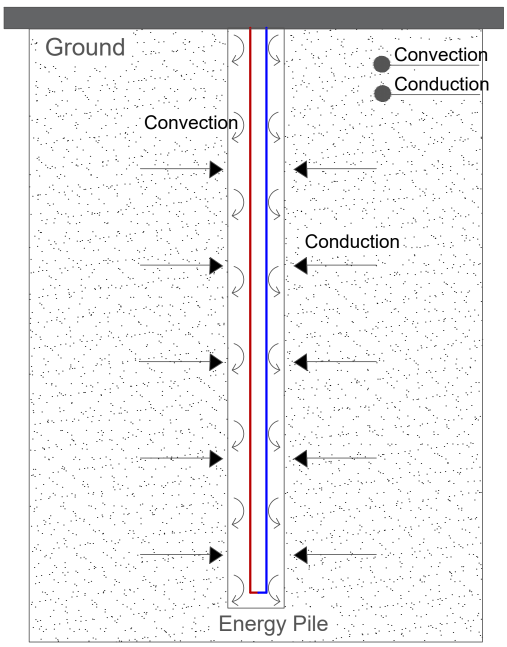

Figure 2.5. Heat transfer modes involved with energy geostructures.

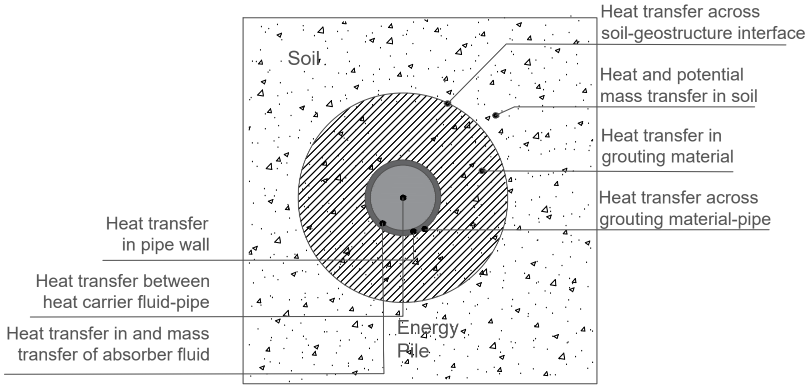

Figure 2.6. Heat transfer mechanism for an energy pile.

2.4.1. Conduction

Conduction is the thermal motion of solid or fluid molecules to transfer heat energy. This motion occurs at the microscopic level and is related to energy diffusion. Physically, conduction can be exemplified by particles moving within a medium bounded by two surfaces at different temperatures. This phenomenon is illustrated in Figure 2.7. The molecules in gases are farther apart than in solids and liquids and have less frequent interactions. Conduction is governed by atomic activity in the form of lattice vibration in solids. Thus, conduction heat transfer is more effective in solids than in fluids.

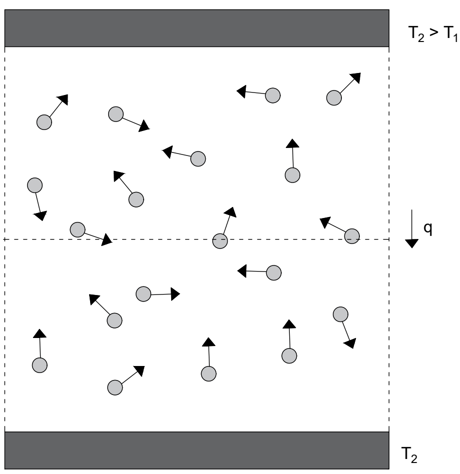

Figure 2.7. Conduction heat transfer.

Conduction is governed by Fourier's law. According to this equation, the amount of heat transferred per unit time across an area, A, is proportional to the area and the negative gradient of temperature, dT/dx. Heat transfer occurs from warmer to cooler material; therefore,

$$q = -kA\frac{dT}{dx} \tag{2.2}$$

where, A is the surface area across which heat is transferred (m^2), k is the thermal conductivity of the solid (W/m·K), q is the rate of heat flow across the area Ab(W), T is temperature (K), and x is the distance normal to the surface A (m), respectively.

2.4.2. Convection

Heat transfer between a fluid and a solid surface is called convection. It is characterized by fluid particles moving in the presence of a temperature gradient. Convection involves both energy transport by diffusion and bulk motion of the fluid. Energy diffusion results from microscopic molecular movements, while bulk motion refers to the macroscopic movement of the fluid. This bulk movement is known as convective mass transfer and is associated with advection. The physical aspect of convection can be explained as fluid motion relative to a bounding surface at different temperatures. This phenomenon is illustrated in Figure 2.8. At the surface, the temperature is T_s, and in the bulk fluid it is $T_\infty < T_s$. Since the wall temperature is higher, heat transfers from the wall to the fluid. At the surface, convection occurs, while molecular diffusion dominates within the fluid boundary layer.

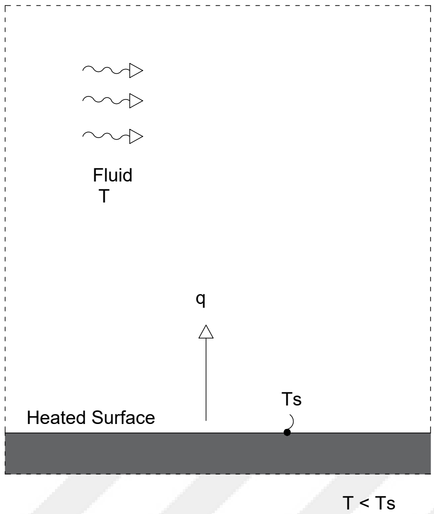

Figure 2.8. Convection heat transfer.

Convection is usually subdivided into two phenomena: natural (free) and forced convection. The temperature difference between materials causes a density difference, which triggers fluid motion. If the bulk fluid motion is caused solely by the thermal gradient, it is called natural convection. Fluid motion caused by any other means is called forced convection. A mixed mode of convection heat transfer arises when both natural and forced convection occur simultaneously.

Convection is governed by Newton's law of cooling. According to this law, the heat flux density is proportional to the temperature difference between the surface and the fluid, with the heat transfer coefficient as the proportionality constant, which can be calculated as

$$q_{\text{conv}} = h_c(T_s - T_f) \tag{2.3}$$

where, q_{conv} is the convective heat flux, T_{s} is the surface temperature, and T_{f} is the fluid temperature, respectively.

2.4.3. Radiation

Radiation is the heat transfer process in which heat waves are emitted by a body. For example, the sun heats the Earth through radiation via electromagnetic waves. Radiation plays a more significant role in gases and vacuums than in solids or liquids. Radiation involves energy transfer between a surface and its surroundings due to temperature differences. This phenomenon is illustrated in Figure 2.9 T_s is the surface temperature, and T_∞ is the constant temperature of the larger surface.

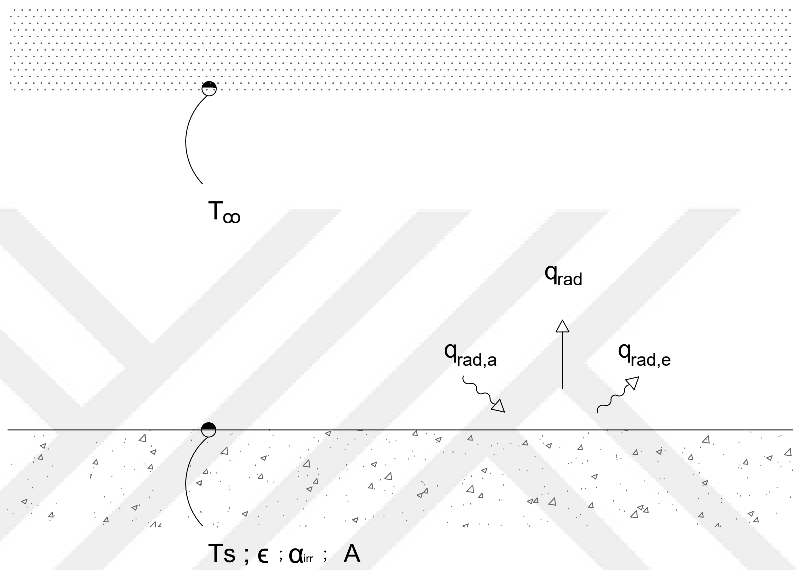

Figure 2.9. Radiation heat transfer.

Radiation is governed by the Stefan-Boltzmann law. According to this law, the heat flux density emitted by a surface depends on the thermal energy of the body bounded by that surface. The equation is expressed as

$$q_{\mathrm{rad},e} = \varepsilon \sigma S_B T_s^4 \tag{2.4}$$

where, ε is the surface emissivity and σ_{SB} is the Stefan–Boltzmann constant equal to 5.67×10^{-8} W/(m^2 K^4).

If the radiation is absorbed from a heat source nearby, the equation changes to

$$q_{\mathrm{rad},e} = \alpha_{\mathrm{irr}} \sigma S_B T_\infty^4 \tag{2.5}$$

where, α_{irr} is the surface absorptivity.

[14] performed a field test and numerical study, concluding that the performance of energy piles as underground solar energy storage is efficient. [15] investigated the

influence of surface solar radiation on the thermal behavior of energy piles and soil. [16] developed a hybrid system coupling a photovoltaic/thermal panel with energy piles to investigate soil thermal balance, revealing that this novel system efficiently utilizes solar and geothermal energy.

2.5. Energy Piles

Energy piles are a specialized type of energy geostructure that has a dual function as a structural foundation and as a heat exchanger enabling thermal energy transfer between the ground and the superstructure. The first function is the conventional load-bearing role that ensures the structural requirements of the building. The second function enables geothermal energy transfer via an integrated heat exchange system. This system includes heat exchanger pipes connected to the steel cage of the pile. The types and configuration of these tubes affect the heat exchange efficiency. [17]

Many studies have been conducted on energy piles, as attention to this subject has increased exponentially in recent years. Full-scale field experiments observing the thermomechanical response of energy piles under the coupled effects of static and thermal loading have been conducted in various regions [18–25]. Pile efficiency has been investigated through different tests [26–30]. Various studies have also focused on the interaction between energy piles and the group effect [31–34].

The development of computer technology provides intelligent models that can be applied to numerical analyses. The heat exchange capacity of energy piles has been investigated through different numerical studies, depending on heat exchanger pipe type [35], pipe configuration [36], flow rate and inlet temperature [37], and characteristics of the heat exchanger fluid [38]. Furthermore, regression analysis [39] and data-driven machine-learning models such as Artificial Neural Networks (ANN) [40], support vector machines [41], random forest [42], and K-Nearest Neighbor Machine Learning (KNN-ML) [43] tools can be employed.

2.6. Geothermal Pavements

The rapid increase in human population and urbanization has created a great demand for transportation. Roads, bridges, pedestrian pathways, and parking lots comprise large areas of infrastructure. Therefore, the utilization of geothermal pavements can significantly improve thermal regulation and energy sustainability in urban areas. They provide a sustainable energy harvesting system, efficient energy use, mitigation of the urban heat island effect, improved pavement lifespan, and contribute to sustainable infrastructure. [44]

A geothermal pavement mainly comprises horizontal heat exchanger pipes embedded under the surface of the conventional pavement at a shallow depth of 1 m to 2 m [45]. Figure 2.10 illustrates the working principle of a geothermal pavement and its components. The primary circuit includes the heat exchanger loops installed within the pavement. The secondary circuit consists of energy piles that transfer heat to or from the ground medium. A water pump may be employed to maintain continuous circulation of the heat carrier fluid.

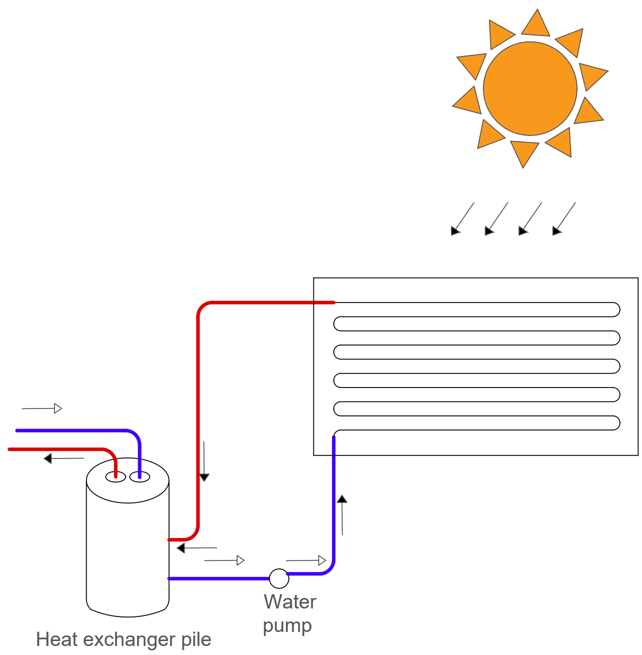

Figure 2.10. Working principle of a geothermal pavement.

The influence of tube spacing and depth on the performance of geothermal pavements has been investigated through various studies [46–49]. Designs that are too shallow or too deep can negatively affect heat exchange and lead to unnecessary costs. The spacing between the heat exchanger pipes should also be considered during design. Baghban (2022) discussed that lower burial depths result in higher temperature gradients, while increased depth reduces solar radiation absorption. The optimal burial depth is proposed to be 40 mm to 60 mm. Pipe spacing is suggested to be in the interval of 5 to 40 cm; shortening the spacing would increase the thermal efficiency of the pavements [50].

The most common usage of geothermal pavements is for snow melting and de-icing. Ice and snow on roads, bridge decks, and pavement slabs cause numerous problems and hazardous road conditions, which are a main cause of accidents and traffic jams during snowy seasons [51]. Therefore, snow melting and de-icing improve traffic safety and reduce accidents. The most commonly used de-icing methods are salting and electrical resistance heaters [52]. These methods are costly and environmentally harmful. Geothermal pavements, on the other hand, are environmentally friendly and cost-effective structures [53]. Horizontal heat exchanger pipes embedded in the pavement maintain the surface temperature above freezing, aiding de-icing [54].

Geothermal pavements are an effective way of utilizing waste heat in urban areas. The urban heat island (UHI) phenomenon, also known as the reverse oasis, occurs due to the accumulation of solar energy during the day [55]. A high concentration of buildings and pavement leads to the formation of heat islands in urban and suburban areas [56]. Heat exchanger pipes embedded in the pavements cool the surface during summer by circulating colder heat carrier fluid, thereby reducing the temperature buildup above the structures. Lower structural temperatures reduce corrosion rates, thereby extending the lifespan of the infrastructure [57].

The newly arising interest in geothermal pavements has caused many studies to be conducted on this novel subject. Different design and modeling approaches have been employed by these studies. Finite Element Models (FEM) have been utilized to simulate and optimize the thermal and mechanical behavior of these structures. [58] developed a numerical model in COMSOL Multiphysics, investigating the long-term performance of a geothermal pavement system. [59] performed a quasi-3D model numerical simulation of horizontal ground coupled heat exchangers. The effects of tube spacing, tube diameter, soil conductivity, and operating conditions were investigated. [60] conducted a numerical analysis using the Midas NFX program to determine the factors affecting the performance of horizontal ground heat exchangers. The performance of geothermal pavement systems was investigated through many field tests. [61] performed a thermal response test (TRT) in order to fill the gaps in our understanding of the thermal behavior of geothermal pavement systems. [62] explored the use of geothermal energy for de-icing in bridge decks through a field-scale experiment.

3. SIMULATION MODEL

3.1. Model Description

A 3D Finite Element model was developed in COMSOL Multiphysics Software v.6.3 to conduct a numerical analysis and investigate the thermal behavior of the geothermal pavement system. Three physics modules were employed. The Heat Transfer in Solids module simulates heat transfer between the ground and the borehole. Heat carrier pipes were modeled via the Heat Transfer in Pipes module. The Pipe Flow module was employed to couple heat transfer and fluid flow. This module simplifies 3D heat exchanger pipes by modeling them as 1D elements.

3.2. Geometry

The model representing the ground is a cylinder with a 10 m radius and an 84 m height. Two different layers were created in the ground model to assign different initial conditions depending on depth, representing natural conditions. The borehole is modeled as another cylinder with a 15.24 cm radius and 60.96 m height, located at the center of the ground. A block with a width of 3.5 m, depth of 1.22 m, and height of 25.4 cm is placed at the surface of the ground. This block represents the pavement. Another block, measuring 6.6 m in width, 25.4 cm in depth, and 25.4 cm in height, is located directly above the borehole, extending towards the pavement. This block was created to embed the heat carrier pipes that connect the borehole to the pavement above the surface. The 3D model view is illustrated in Figure 3.1, and a close-up of the pavement block is presented in Figure 3.2.

Recent studies have assumed the bond between the ground and the borehole to be perfect, without the use of interface elements [63–65]. The same assumption is employed in this study.

Figure 3.1. Overall view of the model.

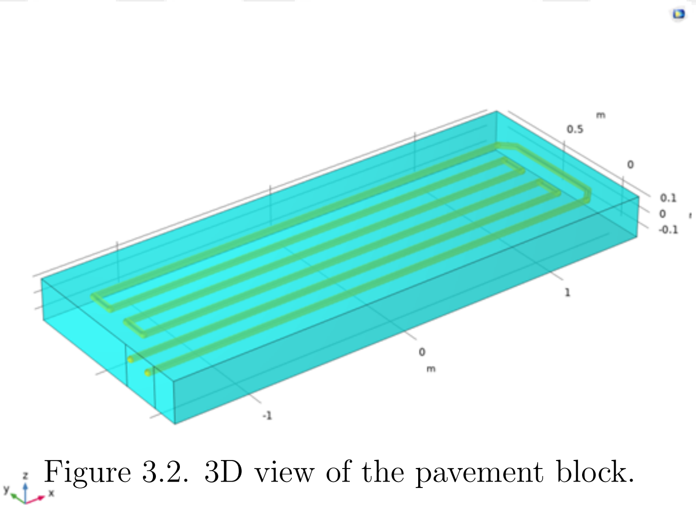

Figure 3.2. 3D view of the pavement block.

Heat carrier pipes are modeled as 1D line elements defined by parametric curves. These edge elements are modeled in the assumed configurations and embedded in three different domains. A single-U configuration is employed in the borehole, while a serpentine configuration is used in the pavement block. Inside the insulation domain, heat carrier pipes are modeled parallel to each other, connecting the two domains. The Heat Transfer in Pipes physics module interface includes parameters for the pipes and the heat carrier fluid. The inner diameters of the pavement pipes are 1.27 cm, and those of the borehole pipes are 3.81 cm. The line elements embedded in the pavement and the borehole are represented in Figure 3.3 and Figure 3.4, respectively.

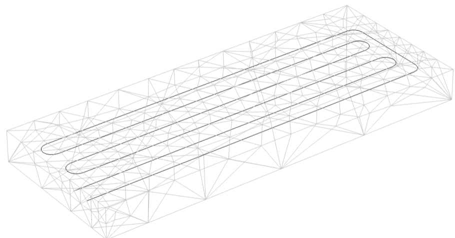

Figure 3.3. 3D view of the pavement and pipes as line elements.

Figure 3.4. 3D view of the borehole and pipes as line elements.

3.3. Materials

The material properties assigned to the domains were chosen to closely represent traditional applications. Ground, borehole, and pavement were modeled as porous media. The ground had a porosity of 0.4, with water filling the voids. The pavement and the borehole was made of concrete with a porosity of 0.1. The voids in concrete were assumed to be filled with air particles. For this study, a multiphase heat carrier fluid, composed of 30% Propylene Glycol (C3H8O2) and 70% water, is circulated in the pipes. The properties of the ground, borehole, and pavement are tabulated in Table 3.1.

Table 3.1. Material properties for ground, borehole, and pavement.

Properties	**Ground**	**Borehole**	**Pavement**
Density, ρ (kg/m^3)	1800	2400	2400
Young's modulus, E (MPa)	25	35000	35000
Poisson's ratio, ν	0.3	0.2	0.2
Porosity, ε	0.4	0.1	0.1
Heat capacity, C_p (J/(kg·K))	900	1000	1000
Thermal conductivity, K (W/(m·K))	1.8	2	2

3.4. Boundary and Initial Conditions

Boundary conditions are coupled within the model using the governing equations; thus, choosing appropriate conditions is crucial to simulate the accurate operation of the model. The far-field and bottom boundaries of the ground are assumed to be sufficiently far away such that no heat transfer occurs through these surfaces. Adiabatic boundary conditions were assigned to these surfaces. The side faces of the pavement were assumed insulated, and thermal insulation boundary conditions were applied.

The top surfaces of the pavement and the ground are assumed to be exposed to climatic conditions. Energy balance boundary conditions were chosen for these surfaces to simulate the effects of heat transfer between the air and the surfaces more realistically. The energy balance boundary condition includes heat transfer via convection, conduction, radiation, solar heating, and precipitation. This was implemented in the model using different modules.The thermal boundary conditions for the ground and pavement models are illustrated in Figures 3.5 and 3.6, respectively.

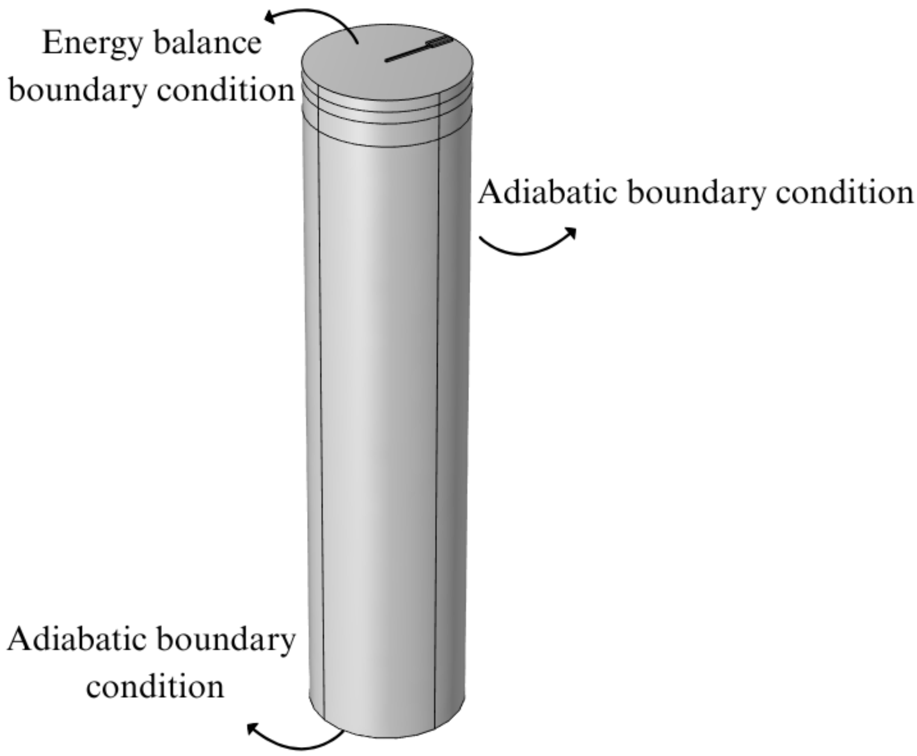

Figure 3.5. Thermal boundary conditions for the ground surfaces.

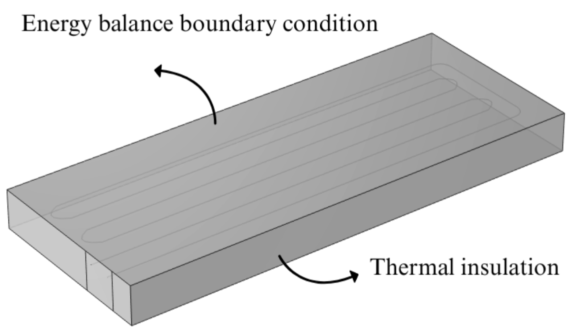

Figure 3.6. Thermal boundary conditions for the pavement surfaces.

The environmental boundary conditions were derived from the climate data of Ankara, a cold and dry city characterized by a continental climate. As the capital of Türkiye and a densely populated urban area, Ankara serves as a representative location where preventing surface icing is particularly important for public safety and energy-efficient infrastructure.

Surface-to-ambient radiation was used to simulate long-wave radiation. The surface emissivity of the pavement is 0.94, while that of the ground surface is 0.96. The wind effect was modeled as a convective heat flux. Short-wave radiation was added as a boundary heat source. The solar absorptivity of the pavement is 0.9, and that of the ground is 0.85. The peak solar irradiance is 600 W/m^2. Precipitation was also modeled as a boundary heat source with a negative sign, representing the energy loss from the surface caused by the phase change of snow. The snowfall rate was taken from meteorological data. The graph showing the snowfall rate in the region from October 1, 2023, to December 31, 2024, is given in Figure 3.7.

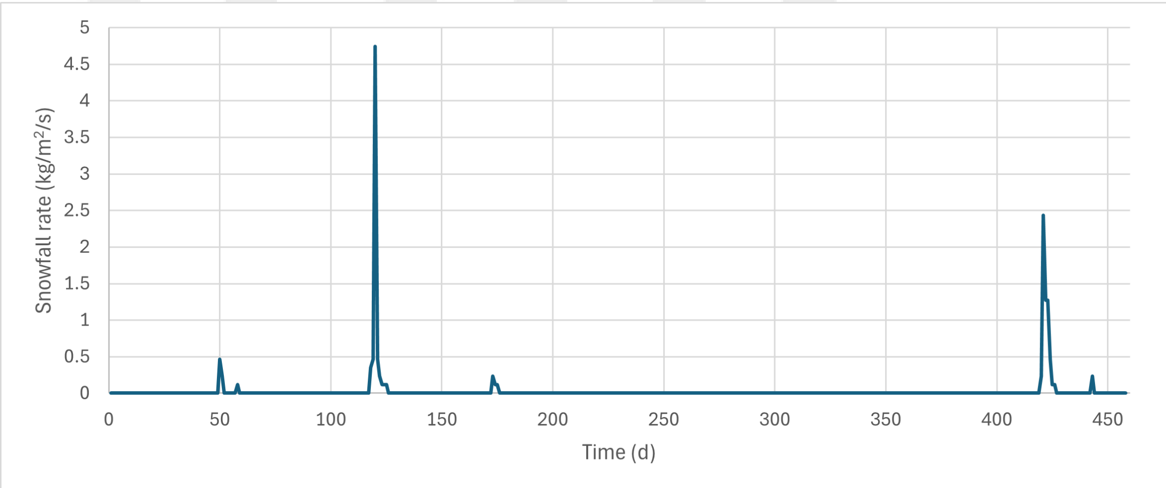

Figure 3.7. Snowfall rate data of Ankara (01.10.2023-31.12.2024).

The initial temperature of the ground varies with depth. In the ground model, two layers were defined. The initial temperatures of the top 1-meter layer, the pavement, and the insulation were all set equal to the ambient air temperature, which is 14°C. The deeper ground temperature was calculated based on the annual average ambient temperature, following the approach in [66], which states that the annual ground temperature is approximately 1.1°C higher than the annual ambient temperature. Accordingly, the annual ambient temperature was taken as 14°C, resulting in a ground temperature of 15.1°C. The monthly ambient temperatures for this city are shown in Figure 3.8.

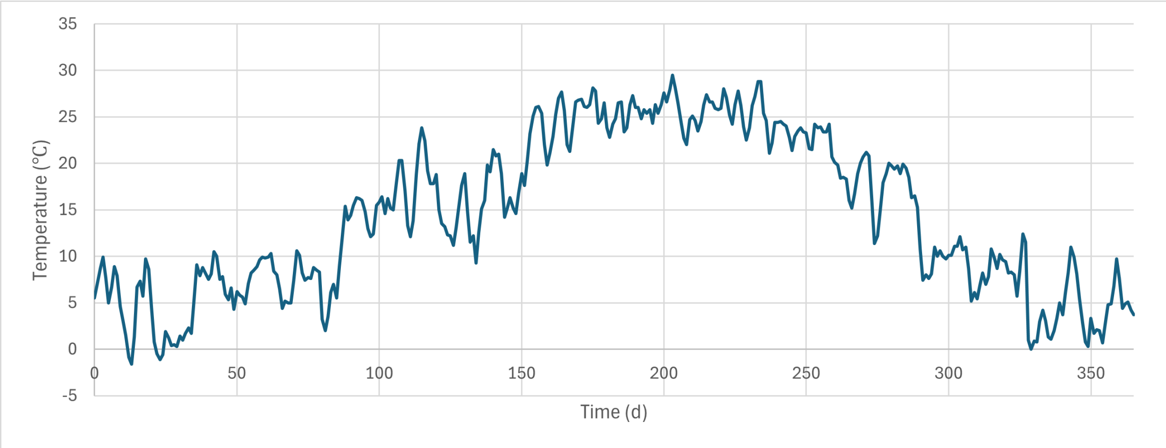

Figure 3.8. Annual ambient temperature of Ankara (01.01.2024-31.12.2024).

3.5. Governing and Constitutive Equations

The formulation is implemented in the model using COMSOL Multiphysics software to accurately calculate the thermal behavior of the system. A time-dependent finite element model was created to simulate the heat transfer between the domains.

The thermal energy change between the porous media is evaluated using the equation

$$(\rho C_p)_{\text{eff}} \frac{\partial T_2}{\partial t} + \rho C_{p,\text{fl}} \mathbf{u} \cdot \nabla T_2 + \nabla \cdot \mathbf{q} = Q + Q_p + Q_{\text{vd}} + Q_{\text{geo}} \tag{3.1}$$

where ρ is the material density, C_p is the specific heat capacity, T is the temperature, t is the time, Q is the general volumetric heat source, Q_p is the work done by pressure forces, Q_{vd} is the viscous dissipation, and Q_{geo} is the geothermal heat source.

Here, q is the heat flux vector, representing the rate and direction of conductive heat transfer. It is governed by Fourier's law. The constitutive equation for q is expressed as

$$\mathbf{q} = -k_{\text{eff}} \nabla T_2 \tag{3.2}$$

where k_{eff} is the effective thermal conductivity of the porous medium.

The first term on the left side of Equation 3.1 describes how temperature changes over time and includes contributions from both solid and fluid phases. The second term represents convective heat transfer caused by the flowing fluid. The last term is the divergence of the heat flux vector, which describes the amount of heat transferred through a point via conduction.

The heat transfer in a heat carrier fluid traveling inside a pipe is calculated by the equation

$$\rho A C_p \frac{\partial T}{\partial t} + \rho A C_p \, \mathbf{u} \cdot \nabla_t T = \nabla_t \cdot (Ak\nabla_t T) + \frac{1}{2}\frac{f_D}{d_h}\rho A|\mathbf{u}|\mathbf{u}^2 + Q + Q_{\text{wall}} \tag{3.3}$$

where, ρ is the material density, A is the pipe cross-sectional area, C_p is the specific heat capacity, T is the temperature, t is the time, $\mathbf{u}$ is the fluid velocity, $\mathbf{e}_t$ is the tangential unit vector, k is the thermal conductivity, f_D is the Darcy friction factor, d_h is the hydraulic diameter, and Q represents the volumetric heat sources within the fluid.

Here, f_{D} is the Darcy friction factor, and it can be calculated with the equations

$$f_D = \begin{cases} \dfrac{64}{Re}, & \text{if } Re < 1000 \\ \max\left(f_{\text{turb}}, \dfrac{64}{Re}\right), & \text{if } Re \geq 1000 \end{cases} \tag{3.4}$$

where, Re is the Reynolds number. It is dimensionless and characterizes the flow regime of a fluid, whether it is laminar, turbulent, or transitional. The definition of this number is calculated as

$$Re = \frac{\rho \, u \, d_h}{\nu} \tag{3.5}$$

where, ρ is the material density, u is the fluid velocity, d_h is the hydraulic diameter, and μ is the dynamic viscosity.

The flow regime is decided through the conditions is expressed as

$$\text{Flow regime} = \begin{cases} \text{Laminar}, & \text{Re} < 2300 \\ \text{Transitional}, & 2300 \leq \text{Re} \leq 4000 \\ \text{Turbulent}, & \text{Re} > 4000. \end{cases} \tag{3.6}$$

Q_{wall} is the rate of heat transferred per unit length of the pipe. It is expressed as

$$Q_{\text{wall}} = (hZ)_{\text{eff}} \cdot (T_{\text{ext}} - T) \tag{3.7}$$

where, $(hZ)_{\text{eff}}$ is the coefficient of effective heat transfer per unit length, T_{ext} is the temperature of the external domain, and T is the temperature of the heat carrier fluid inside the pipe.

The effective heat transfer coefficient models heat conduction and convection in series through a convective layer on the inner pipe wall, conduction across pipe layers (i.e., walls, insulation), and a convective layer at the outer pipe wall. It can be expanded as

$$(hZ)_{\text{eff}} = \frac{1}{\frac{1}{Z_0 h_{\text{int}}} + \frac{1}{Z_N h_{\text{ext}}} + \sum \left(\frac{\ln\left(\frac{r_n}{r_{n-1}}\right)}{2\pi k_{\text{wall},n}} \right)} \tag{3.8}$$

where, Z_0 is the internal wetted perimeter of the pipe, h_{int} is the convective heat transfer coefficient on the internal surface of the pipe, Z_N is the external wetted perimeter of the pipe, h_{ext} is the convective heat transfer coefficient on the external surface of the pipe, r_n is the outer radius of the n-th wall layer, r_{n-1} is the inner radius of the n-th wall layer, and $k_{\text{wall},n}$ is the thermal conductivity of the n-th wall layer.

The first term in the denominator is the internal convection resistance. The second represents the external convection resistance, and the last term is the conduction resistance through each cylindrical pipe wall or insulation layer.

Here, h_{int} can be expanded as

$$h_{\text{int}} = \frac{\text{Nu} \cdot k}{d_h} \tag{3.9}$$

where, d_h is the hydraulic diameter of the pipe, and Nu is the Nusselt number.

Nusselt number is chosen with a condition in order to ensure that the heat transfer is not underestimated. The condition is expressed as

$$\text{Nu} = \max\left(\text{Nu}_{\text{lam}},\ \text{Nu}_{\text{turb}}\right). \tag{3.10}$$

This condition means that the greater value between the laminar and turbulent Nusselt numbers will be used. For circular pipes, the laminar Nusselt number, Nu_{lam}, is 3.66. The turbulent Nusselt number, Nu_{turb}, on the other hand, is calculated using the Gnielinski correlation, which is expressed as

$$\text{Nu}_{\text{turb}} = \frac{\left(\frac{f_D}{8}\right)(Re - 1000)\, Pr}{1 + 12.7\sqrt{\frac{f_D}{8}}\left(Pr^{\frac{2}{3}} - 1\right)}. \tag{3.11}$$

This correlation is valid for

$$\begin{cases} 3000 < Re < 5 \times 10^6, \\ 0.5 < Pr < 2000 \end{cases} \tag{3.12}$$

where, the Prandtl Number, Pr is dimensionless and describes the relative thickness of the momentum and thermal layers. It can be calculated through the equation given as

$$Pr = \frac{C_p \mu}{k} \tag{3.13}$$

where, C_p is the specific heat capacity at constant pressure, μ is the dynamic viscosity, and k is the thermal conductivity.

The working principle of the pump is governed by an equation that relates mass flow rate to velocity at the inlet and outlet of a pipe. This equation assumes a steady-state incompressible flow and no fluid accumulation in the system, and is expressed as

$$u_{\text{in}} = \frac{\dot{m}_{\text{pump}}}{\rho A} = u_{\text{out}} \tag{3.14}$$

where $\dot{m}_{\text{pump}}$ is the mass flow rate of the pump, ρ is the fluid density, A is the cross-sectional area of the pipe, u_{in} is the average velocity at the inlet, and u_{out} is the average velocity at the outlet.

The relationship between the average velocity at the inlet and at the outlet is determined by the cross-sectional areas of the inlet and outlet, assuming constant fluid density.

The energy balance boundary condition applied to the upper surfaces of the ground and pavement is governed by the equation

$$q_0 = q_{\text{conv}} + q_{\text{rad}} + q_{\text{solar}} + q_s \tag{3.15}$$

where, q_0 is the heat flux needed to melt the snow, given by $q_0 = q_{\text{conv}} + q_{\text{rad}} + q_{\text{solar}} + q_s$, with q_{conv} the convective heat flux, q_{rad} the infrared radiation heat flux, q_{solar} the solar radiation heat flux, and q_s the heat flux under the snow.

Convective heat flux considers the wind effect and can be determined as

$$q_{\text{conv}} = h(T_{\text{ext}} - T) \tag{3.16}$$

where, T the surface temperature, T_{ext} the absolute air temperature near the ground, and h the convective heat transfer coefficient. h is expressed as

$$h = \begin{cases} 2 \cdot \dfrac{k_{\text{air}}}{L} \cdot \dfrac{0.3387\, Pr^{1/3} Re_L^{1/2}}{\left(1 + \left(\dfrac{0.0468}{Pr}\right)^{2/3}\right)^{1/4}} & \text{if } Re_L \leq 5 \cdot 10^5 \\ 2 \cdot \dfrac{k_{\text{air}}}{L} \cdot Pr^{1/3}\left(0.037 Re_L^{4/5} - 871\right) & \text{if } Re_L > 5 \cdot 10^5. \end{cases} \tag{3.17}$$

The incoming solar radiation is evaluated through the equation

$$q_{\text{rad}} = \varepsilon \cdot \sigma \cdot \left(T^4 - T_{\text{sky}}^4\right) \tag{3.18}$$

where, ε is the surface emissivity, σ is the Boltzmann constant (5.67×10^{-8} W/m^2 K^4), and T_{sky} is the sky temperature.

The outgoing infrared solar radiation is calculated by the equation

$$q_{\text{solar}} = \alpha \cdot I \tag{3.19}$$

where, α is the absorptivity coefficient and I is the direct radiation incident on a horizontal surface.

The heat flux of snow melting is governed by the equation

$$q_s = m \cdot (H_f + C_{ps}(T_m - T_{\text{snow}})) \tag{3.20}$$

where, m is the mass snowfall rate, H_f is the latent heat of fusion of snow, C_{ps} is the heat capacity of snow, T_m is the melting temperature, and T_{snow} is the snow temperature.

3.6. Events

One of the most important aspects of engineering is creating solutions that are sustainable and economically viable. This requires the system to operate effectively with minimal cost. To achieve this, it is desirable to control the periods during which the geothermal heating system runs. In this work, this is accomplished using a mathematical physics interface called Events in COMSOL. Two different conditions control the state of the pump in the geothermal heating system.

The first condition is applied to control the system for de-icing purposes. As mentioned earlier, the formation of ice and frost on the pavement surface is a primary cause of traffic incidents. The aim here is to prevent this phase change and keep the surface safe at all times. A condition is modeled through a discrete event module, stating that the fluid pump will operate when the average pavement surface temperature falls below the dew point and will stop when the temperature rises to a certain value. The dew point is 7 °C, taken as the average for the winter months (January, February, March, October, November, and December) from meteorological data [67]. The temperature at which the system stops is set with a 9 °C buffer added to the dew point temperature.

The second conditioning prevents the formation of the aforementioned phenomenon, Urban Heat Island. In the literature, it is accepted that when the temperature of the pavement surface is 10 °C higher than the ambient temperature, UHI occurs. Here, the same assumption is made, and two implicit events are created. The pump was set to start working when the pavement surface temperature passes 10℃ above the ambient air temperature, and stops when it drops to 2℃ above the ambient temperature. What this means is that if the pavement starts to accumulate heat on its surface, the system gets triggered to work, and through the circulation of the heat carrier fluid, the excessive heat is transferred to the ground. And later, in order to prevent the overworking of the pump, the system is shut down.

3.7. Meshing

The selection of meshing is critical in finite element modelling as it affects the accuracy, stability, and computational efficiency. A finer mesh gives more accurate results and helps avoid errors like divergence, oscillations, or artificial numerical diffusion, but it also increases the memory use and computation time. Thus, using different element sizes for different domains is the best choice to balance accuracy and time. In this study, the ground domain is meshed with bigger elements, the pavement, borehole, and insulation domains, which contain the pipes with slightly smaller elements, and the heat carrier pipes with the smallest ones. There are 26575 tetrahedral, 3161 triangular, 1774 edge, and 68 vertex elements in this model. The meshing of the entire model is represented in Figure 3.9 and a close op to the surface in Figure 3.10.

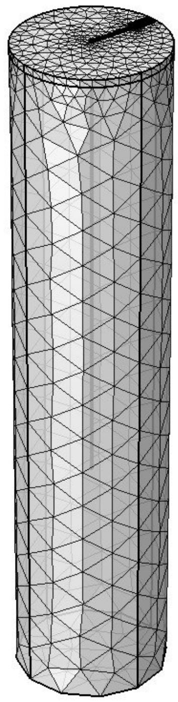

Figure 3.9. Meshing applied to the model.

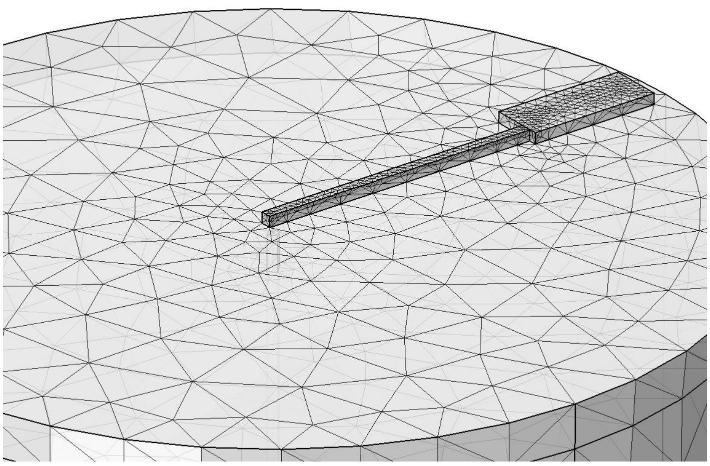

Figure 3.10. Close up of the meshing applied to the model.

4. RESULTS

4.1. Initial Thermal Stabilization Period (0–90 Days)

In order to understand the seasonal behaviour of the system, a full-year simulation was conducted. Additionally, a 90-day period was included at the start of the simulation without system activation. During this stage, the thermal conductivity of the heat exchanger pipes was set to zero. This approach aimed to allow the domains to settle into a stable thermal state. Throughout this phase, the pavement surface was influenced by environmental conditions such as wind, radiation, and precipitation, with an average ambient air temperature of approximately 11°C.

After day 90, the thermal conductivity of the pipes was set to 0.5 W/(m·K). From this point onward, heat transfer was activated between the solid domain and the heat carrier fluid. Figures 4.1, 4.2, 4.3, and 4.4 presents the temperature distribution at four key locations within the model: the pavement surface, the horizontal plane where the embedded pipes are located, and the horizontal cross-section of the ground extending to depths of 1 and 30 meters. The results are shown for five selected time steps—day 0, day 90, day 91, day 180, and day 457—to capture the thermal evolution of the system before activation, immediately after activation, during mid-winter operation, and on the final day.

The figures show the activation of the pipes after the 90th day. Before the activation period, heat is distributed along the planes (Figures a and b). However, a distinct region of temperature difference becomes evident along the serpentine pipes after day 90 (Figure c). This localized thermal change indicates heat transfer between the pavement and the circulating fluid. Despite the heat being confined and not significantly propagating toward the pavement surface, this demonstration proves continued heat transfer (Figures d and e).

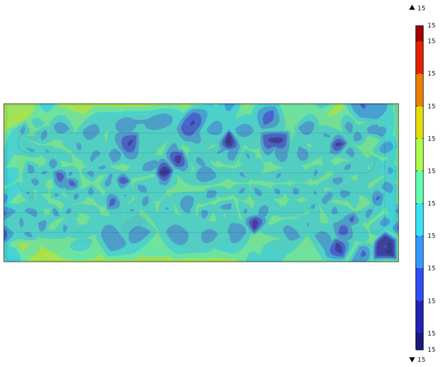

(a)

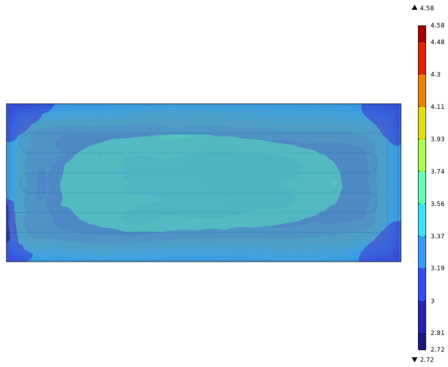

(b)

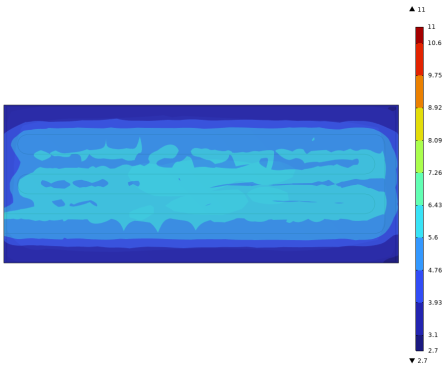

(c)

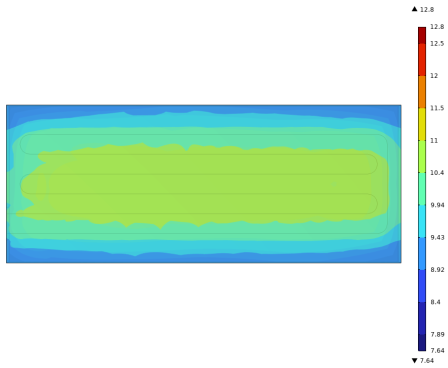

(d)

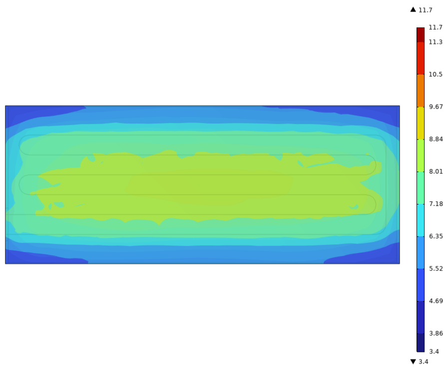

(e)

Figure 4.1. Temperature distribution in the pavement surface at (a) day 0,(b) day 90, (c) day 91, (d) day 180, and (e) day 457.

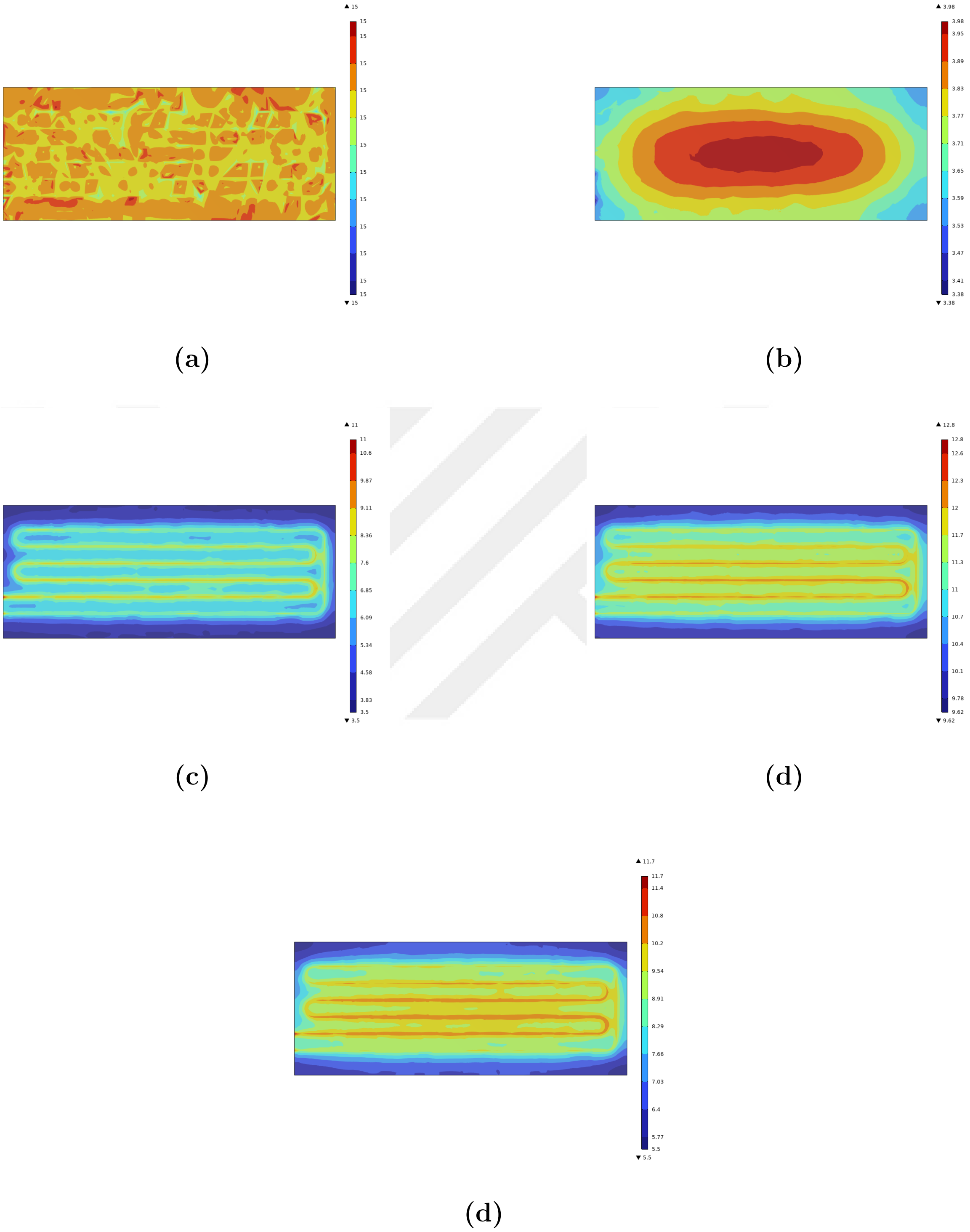

Figure 4.2. Temperature distribution in the pavement layer at the depth of the horizontal pipes at various times: (a) day 0, (b) day 90, (c) day 91, (d) day 180, and (e) day 457.

Figure 4.3 and Figure 4.4 depict the temperature distribution through the horizontal cross-section of the ground at 1 and 30 meters. To assess the effect of environmental conditions on heat transfer, the thermal distribution at two different depths was extracted. While the 1 m layer of the ground is exposed to climatic conditions throughout the year, at 30 m depth the annual temperature remains stable.

These slices show that during the 90-day starting period, the temperature distribution is uniform and not influenced by the energy pile (Figures a and b). The energy pile is activated starting from day 91, and a region of heat transfer becomes visible (Figure c). The continuity of heat extraction is evident from the expansion of thermal change (Figures d and e). The radial symmetry of the temperature gradient suggests that the energy pile acts as a central heat source.

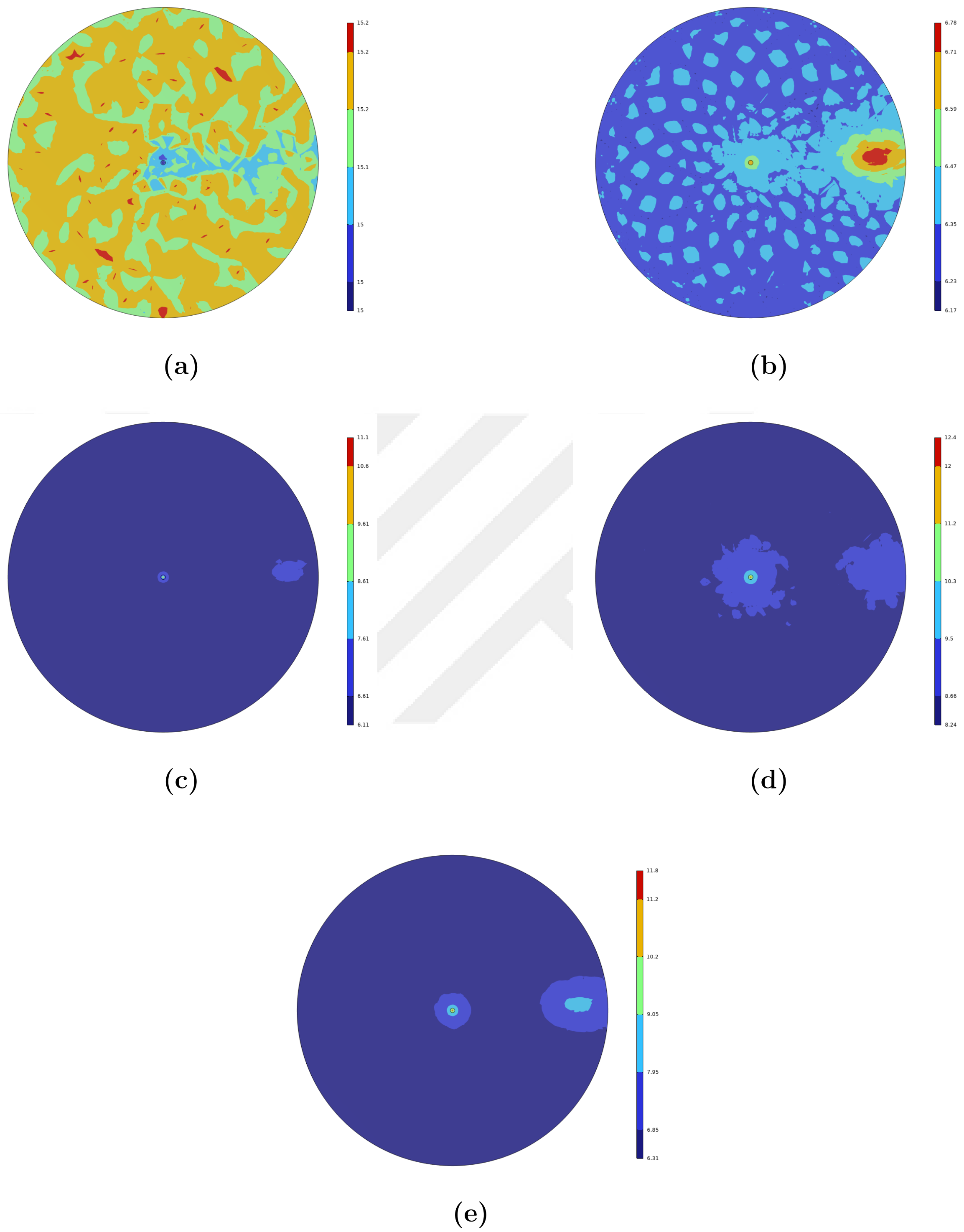

Figure 4.3. Temperature distribution in the ground at 1 m depth at (a) day 0, (b) day 90, (c) day 91, (d) day 180, and (e) day 457.

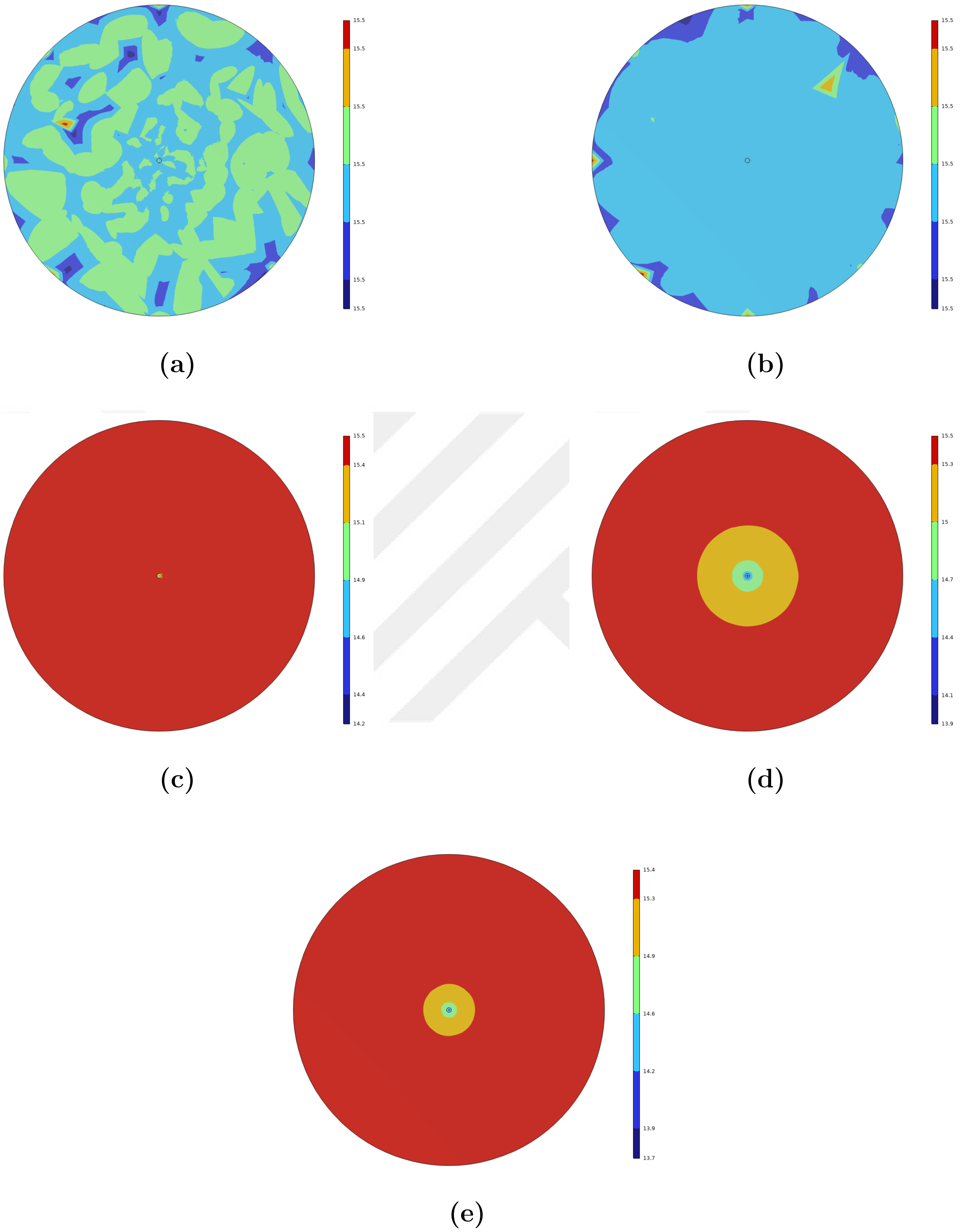

Figure 4.4. Temperature distribution in the ground at 30 m depth at (a) day 0, (b) day 90, (c) day 91, (d) day 180, and (e) day 457.

4.2. Effectiveness of the System on Pavement Surface Temperature

After the 90-day inactive period, the geothermal system was activated, and heat transfer from the subsurface to the pavement was enabled. The main aim of the study was to prevent the surface temperature of the pavement from dropping below 7°C. Two scenarios were compared to investigate the effectiveness of the heating system: when the system is at rest and when it is running. The comparison is shown in Figure 4.5.

As reflected in the plot, for both scenarios, temperatures follow a similar path while the system was inactive. On day 91, a sudden temperature rise can be seen in the system activation scenario. This spike highlights the effect of the geothermal system as soon as circulation starts.

In the inactive scenario, during winter conditions—particularly from day 90 to approximately day 180—the pavement temperature drops below 7°C, reaching a minimum of 1°C. These low temperatures indicate the risk of ice formation on the surface. However, during the active scenario, the pavement surface temperature is maintained above 7°C, demonstrating the system's heating capacity and frost prevention potential.

Following the winter period, the stabilizing effect of the system can be observed. In the inactive scenario, the surface temperature fluctuates sharply due to its high sensitivity to climatic conditions. A comparison of ambient air temperature and pavement surface temperature for the same period is presented in Figure 4.6. It can be seen from the graph that there is a correlation between low ambient temperatures and drops in pavement surface temperature in the inactive heating system state. The geothermal system, however, smooths these reactions and moderates the thermal changes. Toward the end of the simulation, after day 400, another winter season begins. Again, in the inactive scenario, the surface temperature tends toward lower values, while the active system continues to preserve higher thermal stability.

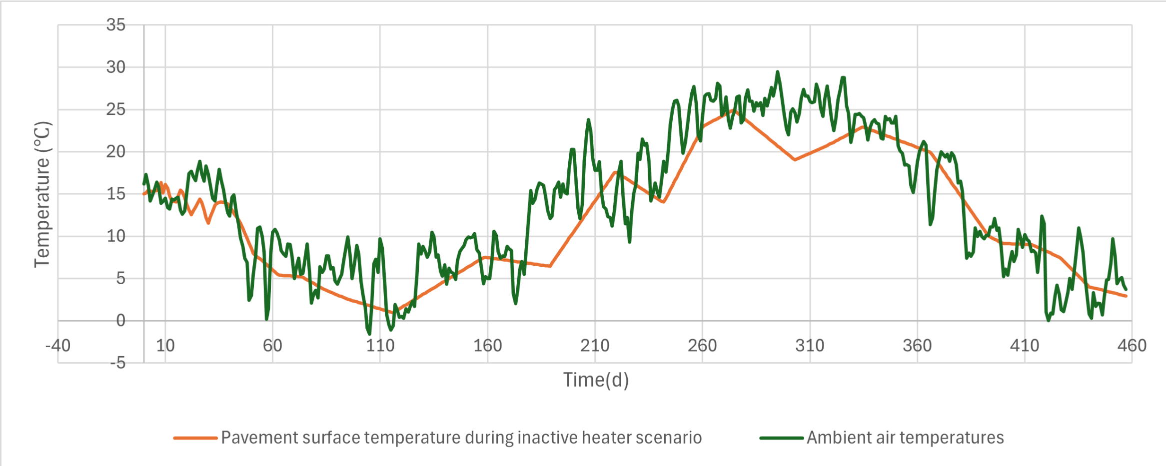

Figure 4.5. Comparison of ambient air temperature and the temperature profiles at the pavement surface over time in the inactive scenario.

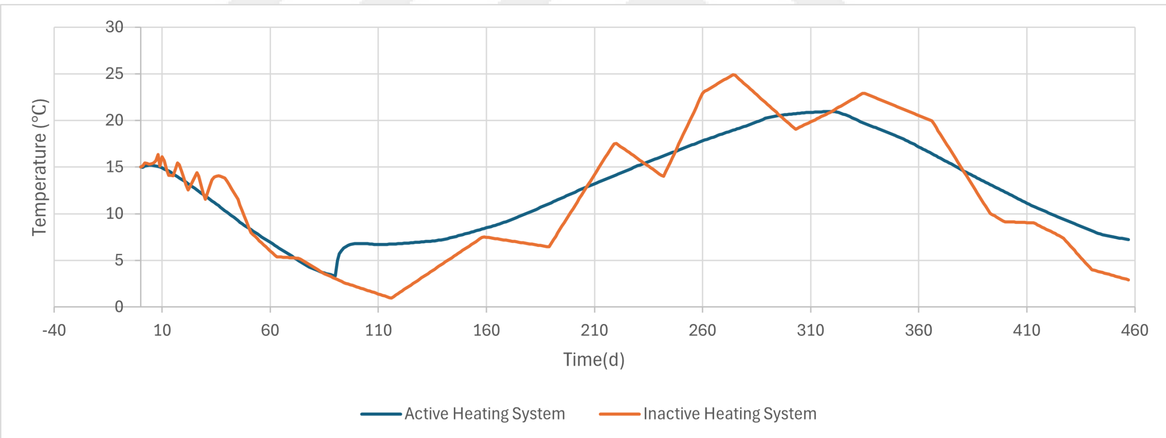

Figure 4.6. Temperature profiles at the pavement surface over time during heating system active and inactive scenarios.

4.3. Performance Under Event-Based Operation

An event-based logic was implemented in the model to improve energy efficiency and prevent overworking of the system. This was achieved using the Events interface in COMSOL Multiphysics. The first step in this operation was selecting a threshold value to trigger system activation. To fulfill the aim of this study, the pavement surface had to be maintained above a certain temperature to prevent ice formation. This threshold was determined based on a review of historical weather conditions. The maximum dew point temperature during snow events was 6.4°C. Therefore, a threshold of 7°C was chosen to activate the heating system, ensuring proactive frost prevention under worst-case dew point conditions.

Figure 4.7 illustrates the average pavement surface temperature and the pump state over the 457-day simulation period. The pump was triggered to work four times during the year, primarily in January, February, and March. Despite the pump not working throughout the entire year, the system managed to keep the pavement surface above 7 °C. Compared to a continuously active system, this approach significantly reduced the total amount of heat the system had to deliver and the potential energy consumption, while still achieving the primary performance goal.

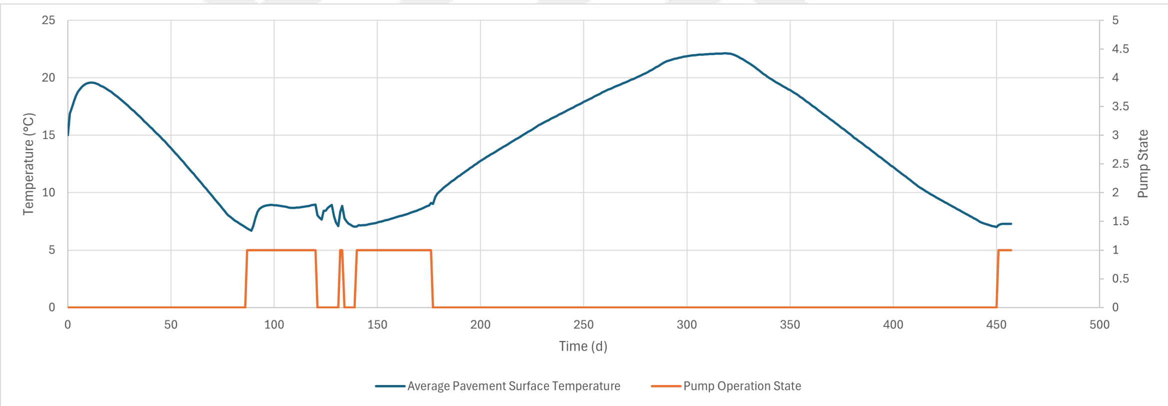

Figure 4.7. The activation of the pump depending on the average pavement surface temperature.

5. DISCUSSIONS

5.1. Interpretation of Results

The results presented in this chapter underline the performance of the geothermal pavement system across different operational phases. In order to ensure a reliable baseline, an initial thermal stabilization period was added to the simulation. This period allowed the model to reach thermal steady-state conditions.Overall, these findings confirm the systems' potential for sustainable and efficient pavement temperature management.

Later, during the active phases, the system maintained the pavement surface temperature above freezing, demonstrating its capability to prevent ice formation. The control mechanism further optimized energy consumption, allowing the pump to work only when necessary, without compromising thermal performance.

The Urban Heat Island Effect mitigation strategy was included to the system to prevent overheating of the pavement. However, under the climatic conditions used in the model, this mechanism is never triggered. This indicates that the pavement remains in moderate temperatures during warmer seasons and does not exacerbate urban warming.

5.2. Limitations and Model Assumptions

When discussing the results, limitations should be considered. A homogeneous soil domain and steady boundary conditions were assumed by the model. These assumptions do not reflect the real field conditions of heterogeneous soil and variable weather patterns.

The treshold temperatures selected for the event-based control mechanism are predifinded and may requiere redifenment based on real-time monitoring.

The simulation simplifies the complex interactions between the pavement, the ground and the climatic conditions. This can affect the long-term behaviour of the system. A more detailed weather data, soil layering, and dynamic boundary conditions can enhance model realibility.

5.3. Practical Implications and Future Work

The simulations results indicate that geothermal pavement systems with event-based controls has the adequate potential to prevent ice formation while minimizing energy consumption. This suggests a promising pathway for integrating sustainable thermal management solutions in cold urban environments.

Future studies should focus on field validation of the model and adaptive control algorithms that responds to real-time temperature and weather data. The efficiency of the model can be tested under altered versions such as with multiple boreholes, different pipe configurations and material properties, and varying soil conditions.

6. CONCLUSION

This study aimed to evaluate the thermal performance of a geothermal pavement system through numerical simulation. COMSOL Multiphysics Software 6.3 was employed, and the Heat Transfer in Solids, Heat Transfer in Pipes, and Pipe Flow physics modules were incorporated. Winter conditions were taken into consideration to focus on the prevention of ice formation. A closed-loop pipe system with a pump was modeled to investigate the heat transfer efficiency between the ground and the pavement. Environmental conditions were applied as boundary conditions. An event-based pump control system was implemented to reduce energy consumption.

The simulation was conducted over a period of 457 days. An initial 90-day period was modeled to allow the ground and the pavement to reach thermal equilibrium. During this phase, the geothermal heating system was inactive, and there was no heat transfer between the circulating fluid and the surrounding domains. After 90 days, the system was activated, and heat transfer was allowed. This approach enabled the observation of both the transient ground behavior and the effectiveness of system activation under winter conditions.

Cross-sectional views of the ground at different depths confirmed the influence of climatic variations on shallow ground layers. At a depth of 30 meters, the ground temperature remained stable throughout the year, while the first meter was more responsive to environmental conditions. This behavior validated the need to monitor surface-level conditions for ice risk assessment. Furthermore, the cross-sectional views at different time steps confirmed that, during the initial phase, heat remained confined around the pipes but gradually dispersed into the ground and the pavement.

Comparative analysis of the active and inactive heating scenarios showed that, in the absence of heating, the pavement surface temperature dropped to 1°C, entering the critical range for frost and ice development. In contrast, the active system successfully maintained surface temperatures above 7°C throughout the winter season.

The operation of the pump was controlled by an event-based trigger mechanism. The system was activated only when the pavement surface temperature dropped below 7°C. This threshold was derived from historical dew point data during snow events. The results demonstrated that the system responded as designed to low-temperature events.

Additionally, the urban heat island effect was taken into consideration. Due to solar radiation and heat accumulation, the surface temperature can rise above ambient levels. Another event-based control mechanism was implemented during the summer months to prevent pavement overheating and initiate a cooling cycle. However, it was observed that the temperature did not reach the threshold, so the system was not activated.

Overall, the numerical study successfully demonstrated that the geothermal pavement system is effective and functions as intended. The integration of the event-based control system enabled stable and safe pavement temperatures while maintaining energy efficiency. The study shows that such systems can offer a sustainable solution for frost prevention in urban infrastructure.

REFERENCES

1. Soltani, M., F. M. Kashkooli, A. R. Dehghani-Sanij, A. Nokhosteen, A. Ahmadi-Joughi, K. Gharali, S. B. Mahbaz and M. B. Dusseault, "A Comprehensive Review of Geothermal Energy Evolution and Development", *International Journal of Green Energy*, Vol. 16, No. 13, pp. 971–1009, 2019.

2. Ragheb, M., *Terrestrial Radioactivity and Geothermal Energy*, Lecture notes, University of Illinois, Nuclear Power Engineering, Urbana-Champaign, IL, USA, 2019.

3. Kusuda, T. and P. R. Achenbach, *Earth Temperature and Thermal Diffusivity at Selected Stations in the United States*, Technical Report NBS Report 8972, National Bureau of Standards, Gaithersburg, MD, USA, 1965.

4. Barbier, E., "Geothermal Energy Technology and Current Status: An Overview", *Renewable and Sustainable Energy Reviews*, Vol. 6, No. 1, pp. 3–65, 2002.

5. Sharmin, T., N. R. Khan, M. S. Akram and M. M. Ehsan, "A State-of-the-Art Review on Geothermal Energy Extraction, Utilization, and Improvement Strategies: Conventional, Hybridized, and Enhanced Geothermal Systems", *International Journal of Thermofluids*, Vol. 18, p. 100323, 2023.

6. Laloui, L. and A. F. Rotta Loria, *Energy and Geotechnologies*, pp. 3–23, Elsevier, Amsterdam, Netherlands, 2020.

7. Brandl, H., "Energy Foundations and Other Thermo-Active Ground Structures", *Géotechnique*, Vol. 56, No. 2, pp. 81–122, 2006.

8. Florides, G. and S. Kalogirou, "Ground Heat Exchangers: A Review of Systems, Models, and Applications", *Renewable Energy*, Vol. 32, No. 15, pp. 2461–2478, 2007.

9. Luo, J., H. Zhao, S. Gui, W. Xiang, J. Rohn and P. Blum, "Thermo-Economic Analysis of Four Different Types of Ground Heat Exchangers in Energy Piles", *Applied Thermal Engineering*, Vol. 108, No. C, pp. 11–19, 2016.

10. Zaim, E. H., H. Farzan and M. Ameri, "Assessment of Pipe Configurations on Heat Dynamics and Performance of Pavement Solar Collectors: An Experimental and Numerical Study", *Sustainable Energy Technologies and Assessments*, Vol. 37, p. 100635, 2020.

11. Banks, D., *An Introduction to Thermogeology: Ground Source Heating and Cooling*, Wiley-Blackwell, Chichester, United Kingdom, 2012.

12. BS EN 14825, *Air Conditioners, Liquid Chilling Packages and Heat Pumps, with Electrically Driven Compressors, for Space Heating and Cooling, Commercial and Process Cooling: Testing and Rating at Part Load Conditions and Calculation of Seasonal Performance*, British Standards Institution, London, United Kingdom, 2022.

13. Rotta Loria, A. F., "Energy Geostructures: Theory and Application", J. S. McCartney and I. Tomac (Editors), *E3S Web of Conferences*, Vol. 205, p. 01004, La Jolla, California, USA, 2020.

14. Wu, D., G. Kong, H. Liu, Q. Jiang, Q. Yang and L. Kong, "Performance of a Full-Scale Energy Pile for Underground Solar Energy Storage", *Case Studies in Thermal Engineering*, Vol. 27, p. 101313, 2021.

15. Polat, S., M. Guner, U. C. Erginag, M. Sutman and O. Cinicioglu, "Analyses of Thermoactive Piles Considering Surface Radiation and Wind Convection Effects", *International Journal of Geomechanics*, Vol. 25, No. 1, p. 04024310, 2025.

16. Wang, F. and T. You, "Synergetic Performance Improvement of a Novel Building Integrated Photovoltaic/Thermal–Energy Pile System for Co-Utilization of Solar and Shallow-Geothermal Energy", *Energy Conversion and Management*, Vol. 288,

p. 117116, 2023.

17. Chen, S., Y. Deng, S. Niu, W. Ming, G. Chen and R. Zhang, "Finite Element Analysis of Combined Energy Piles With Long and Short Heat Exchanger Tubes", *Applied Sciences*, Vol. 13, No. 23, p. 12579, 2023.

18. Chen, Z., Y. Sun, H. Xiao, Q. Ma and L. Zhang, "In-Situ Thermomechanical Response Test of an Energy Pile Under Temperature Loading", *Arabian Journal for Science and Engineering*, Vol. 46, No. 11, pp. 10355–10364, 2021.

19. Feng, S., J. Fang, Y. Zhao, Z. Zhang and Y. Wang, "Thermomechanical Analysis of Energy Piles Using a Load-Transfer Approach Considering Soil Coupling Effects", *Computers and Geotechnics*, Vol. 168, p. 106147, 2024.

20. Ghezellou, A., M. Keramati and O. Ghasemi-Fare, "Thermomechanical Response of Energy Piles in Dry Sand Under Monotonic Cooling With Varying End-Support Conditions", *Journal of Energy Storage*, Vol. 82, p. 110469, 2024.

21. Jiang, G., C. Lin, D. Shao, M. Huang, H. Lu, G. Chen and C. Zong, "Thermo-Mechanical Behavior of Driven Energy Piles From Full-Scale Load Tests", *Energy and Buildings*, Vol. 233, p. 110668, 2021.

22. Markiewicz, R., A. T. Brunner, J. Pistrol and D. Adam, "Field Investigations on the Thermo-Mechanical Behavior of a Partially Activated Energy Pile in Miocene Sediments", *Geomechanics for Energy and the Environment*, Vol. 40, p. 100605, 2024.

23. Rafai, M., D. Salciarini and P. J. Vardon, "Energy Pile Displacements Due to Cyclic Thermal Loading at Different Mechanical Load Levels", *Acta Geotechnica*, Vol. 20, No. 6, pp. 3067–3086, 2025.

24. Ren, L.-W., Z.-P. Han, J.-W. Huo and Y.-J. Gao, "Feasibility Analysis of Low Thermal Conductivity Asphalt Concrete Bridge Deck Deicing by Using Geothermal

Energy", *IOP Conference Series: Earth and Environmental Science*, Vol. 861, p. 032090, IOP Publishing, Bristol, England, 2021.

25. Wang, Y., F. Zhang, F. Liu and X. Wang, "Full-Scale In Situ Experimental Study on the Bearing Capacity of Energy Piles Under Varying Temperature and Multiple Mechanical Load Levels", *Acta Geotechnica*, Vol. 19, No. 1, pp. 401–415, 2024.

26. Ateş, B. and E. Şadoğlu, "Experimental Investigation for Group Efficiency of Driven Piles Embedded in Cohesionless Soil", *KSCE Journal of Civil Engineering*, Vol. 27, No. 12, pp. 5123–5134, 2023.

27. Cecinato, F. and F. A. Loveridge, "Influences on the Thermal Efficiency of Energy Piles", *Energy*, Vol. 82, pp. 1021–1033, 2015.

28. Hamada, Y., H. Saitoh, M. Nakamura, H. Kubota and K. Ochifuji, "Field Performance of an Energy Pile System for Space Heating", *Energy and Buildings*, Vol. 39, No. 5, pp. 517–524, 2007.

29. Hamid, A., W. M. Hamid and A. M. Alnuaim, "Factors Affecting Energy Pile Efficiency", *Soil Mechanics and Foundation Engineering*, Vol. 58, No. 4, pp. 302–307, 2021.

30. He, F., C. Wang, A. Bouazza, G. Kong and Z. Sun, "Investigation on Thermal Performance of Energy Pile and Borehole Heat Exchanger Under Intermittent Field Operating Conditions", *Energy and Buildings*, Vol. 320, p. 114643, 2024.

31. Kong, G., H. Chang, D. Wu, H. Peng, Y. Shen and H. Abuel-Naga, "Effects of Pile Configuration on the Group Behavior of Semi-Floating Energy Piles", *Journal of Building Engineering*, Vol. 77, p. 107487, 2023.

32. Rotta Loria, A. F. and L. Laloui, "Thermally Induced Group Effects Among Energy Piles", *Geotechnique*, Vol. 67, No. 5, pp. 374–393, 2017.

33. Sailauova, D., Z. Mamesh, D. Zhang, D. Lee, C. S. Shon and J. R. Kim, "Group Pile Effect on Temperature Distributions Inside Energy Storage Pile Foundations", *Applied Sciences*, Vol. 10, No. 18, p. 6597, 2020.

34. Yin, Y., Q. Li and L. Qiao, "Response of Energy Pile-Soil Structure and Pile Group Effect: An Indoor Similarity Simulation Study", *Journal of Building Engineering*, Vol. 51, p. 104247, 2022.

35. Gashti, E. H. N., V. M. Uotinen and K. Kujala, "Numerical Modelling of Thermal Regimes in Steel Energy Pile Foundations: A Case Study", *Energy and Buildings*, Vol. 69, pp. 165–174, 2014.

36. Mehrizi, A. A., S. Porkhial, B. Bezyan and H. Lotfizadeh, "Energy Pile Foundation Simulation for Different Configurations of Ground Source Heat Exchanger", *International Communications in Heat and Mass Transfer*, Vol. 70, pp. 105–114, 2016.

37. Gao, J., X. Zhang, J. Liu, K. Li and J. Yang, "Numerical and Experimental Assessment of Thermal Performance of Vertical Energy Piles: An Application", *Applied Energy*, Vol. 85, No. 10, pp. 901–910, 2008.

38. Akbari Garakani, A., S. Mokhtari Jozani, P. Hashemi Tari and B. Heidari, "Effects of Heat Exchange Fluid Characteristics and Pipe Configuration on the Ultimate Bearing Capacity of Energy Piles", *Energy*, Vol. 248, p. 123583, 2022.

39. You, S., X. Cheng, H. Guo and Z. Yao, "Experimental Study on Structural Response of CFG Energy Piles", *Applied Thermal Engineering*, Vol. 96, pp. 640–651, 2016.

40. Deb, C., L. Siew Eang, J. Yang and M. Santamouris, "Forecasting Diurnal Cooling Energy Load for Institutional Buildings Using Artificial Neural Networks", *Energy and Buildings*, Vol. 121, No. 6, pp. 284–297, 2016.

41. Zhang, X., E. Wang, L. Liu and C. Qi, "Machine Learning-Based Performance Prediction for Ground Source Heat Pump Systems", *Geothermics*, Vol. 105, p. 102509, 2022.

42. Lu, S., Q. Li, L. Bai and R. Wang, "Performance Predictions of Ground Source Heat Pump System Based on Random Forest and Back Propagation Neural Network Models", *Energy Conversion and Management*, Vol. 197, p. 111864, 2019.

43. Priyadarshi, G. and B. K. Naik, "Desiccant Coated Fin Tube Energy Exchanger Design Optimization Implementing KNN-ML Tool and Adsorption/Desorption Kinetics Analysis Using Finite Difference Based Transient Model", *International Journal of Thermal Sciences*, Vol. 192, p. 107498, 2023.

44. Ghorbani, B., A. Arulrajah, G. A. Narsilio, S. Horpibulsuk and A. Buritatum, "Geothermal Pavements: Experimental Testing, Prototype Testing, and Numerical Analysis of Recycled Demolition Wastes", *Sustainability*, Vol. 15, No. 3, p. 2680, 2023.

45. Al-Ameen, Y., A. Ianakiev and R. Evans, "Thermal Performance of a Solar Assisted Horizontal Ground Heat Exchanger", *Energy*, Vol. 140, pp. 1216–1227, 2017.

46. Pu, L., L. Xu, D. Qi and Y. Li, "Structure Optimization for Horizontal Ground Heat Exchanger", *Applied Thermal Engineering*, Vol. 136, pp. 131–140, 2018.

47. Rees, S. J., J. D. Spitler and X. Xiao, "Transient Analysis of Snow-Melting System Performance", *ASHRAE Transactions*, Vol. 108, No. 2, pp. 406–423, 2002.

48. Selamat, S. B., "Numerical Modelling for Horizontal Ground Heat Exchangers Optimization", Master's Thesis, Universiti Teknologi Malaysia, 2016.

49. Zheng, X., Z. Song and Y. Ding, "Heat Exchange Characteristics of Underground and Pavement Buried Pipes for Bridge Deck Heating Conditions", *Plos One*, Vol. 19, No. 5, p. e0298077, 2024.

50. Ghalandari, T., N. Hasheminejad, W. Van den Bergh and C. Vuye, "A Critical Review on Large-Scale Research Prototypes and Actual Projects of Hydronic Asphalt Pavement Systems", *Renewable Energy*, Vol. 177, No. C, pp. 1421–1437, 2021.

51. Musey, K. and S. Park, "Pavement Skid Number and Horizontal Curve Safety", *Procedia Engineering*, Vol. 145, pp. 828–835, 2016.

52. Eugster, W. J., "Proceedings European Geothermal Congress", Technical Report, 2007.

53. Aresti, L., P. Christodoulides and G. Florides, "A Review of the Design Aspects of Ground Heat Exchangers", *Renewable and Sustainable Energy Reviews*, Vol. 92, pp. 757–773, 2018.

54. Mohammadzadeh, A., O. Ghasemi-Fare and Z. Sun, "Enhancing Infrastructure Resilience Through Shallow Geothermal Energy: A Novel Approach to Mitigate Extreme Weather Impacts on Existing Bridges", Technical Report, University of Louisville, 2025.

55. Phelan, P. E., K. Kaloush, M. Miner, J. Golden, B. Phelan, H. Silva and R. A. Taylor, "Urban Heat Island: Mechanisms, Implications, and Possible Remedies", *Annual Review of Environment and Resources*, Vol. 40, pp. 285–307, 2015.

56. Ibrahim, S. H., N. I. A. Ibrahim, J. Wahid, N. A. Goh, D. R. A. Koesmeri and M. N. M. Nawi, "The Impact of Road Pavement on Urban Heat Island (UHI) Phenomenon", *International Journal of Technology*, Vol. 9, No. 8, pp. 1597–1608, 2018.

57. Al-Atroush, M. E., A. Marouf, M. Aloufi, M. Marouf, T. A. Sebaey and Y. E. Ibrahim, "Structural Performance Assessment of Geothermal Asphalt Pavements: A Comparative Experimental Study", *Sustainability (Switzerland)*, Vol. 14, No. 19, p. 12855, 2022.

58. Motamedi, Y., N. Makasis, X. Gu, G. A. Narsilio, A. Arulrajah and S. Horpibulsuk, "Numerical Investigation of Geothermal Pavements: Design Optimisation & Boundary Conditions", *Transportation Geotechnics*, Vol. 33, p. 100785, 2022.

59. Benazza, A., E. Blanco, M. Aichouba, J. L. Río and S. Laouedj, "Numerical investigation of horizontal ground coupled heat exchanger", *Energy Procedia*, Vol. 6, pp. 29–35, Elsevier, Amsterdam, Netherlands, 2011.

60. Kim, M. J., S. R. Lee, S. Yoon and G. H. Go, "Thermal performance evaluation and parametric study of a horizontal ground heat exchanger", *Geothermics*, Vol. 60, pp. 134–143, 2016.

61. Motamedi, Y., N. Makasis, A. Arulrajah, S. Horpibulsuk and G. Narsilio, "Thermal Performance of the Ground in Geothermal Pavements", *Proceedings of the 2nd International Conference on Energy Geotechnics (ICEGT 2020)*, Vol. 205 of *E3S Web of Conferences*, p. 06015, EDP Sciences, Adelaide, Australia, 2020.

62. Mohammadzadeh, A., O. Ghasemi-Fare, Z. Sun and M. McGinley, "Exploring the Use of Geothermal Piles as an Environmentally Sustainable Method to De-Ice Bridge Decks through Field-Scale Experiment", *Proceedings of the Geo-Congress 2024: Soil Improvement, Sustainability, Geoenvironmental, and Cold Regions Engineering*, pp. 751–759, American Society of Civil Engineers (ASCE), Reston, VA, USA, Feb. 2024.

63. Gawecka, K. A., D. M. G. Taborda, D. M. Potts, W. Cui, L. Zdravković and M. S. H. Haji Kasri, "Numerical modelling of thermo-active piles in London Clay", *Proceedings of the Institution of Civil Engineers: Geotechnical Engineering*, Vol. 170, No. 3, pp. 201–219, 2017.

64. Moradshahi, A., M. Faizal, A. Bouazza and J. S. McCartney, "Thermomechanical Responses of Thermally Interacting Field-Scale Energy Piles", *International Journal of Geomechanics*, Vol. 22, No. 11, p. 04022154, 2022.

65. Salciarini, D., F. Ronchi and C. Tamagnini, "Thermo-Hydro-Mechanical Response of a Large Piled Raft Equipped with Energy Piles: A Parametric Study", *Acta Geotechnica*, Vol. 12, No. 4, pp. 703–728, 2017.

66. Ozyurt, O. and D. A. Ekinci, "Experimental Study of Vertical Ground-source Heat Pump Performance Evaluation for Cold Climate in Turkey", *Applied Energy*, Vol. 88, No. 4, pp. 1257–1265, 2011.

67. Visual Crossing, 2025, "Weather Data API", `https://www.visualcrossing.com/weather-api`, Accessed on: June 24, 2025.